JAK2 mutant hematopoietic cells display metabolic alterations that can be targeted to treat myeloproliferative neoplasms

Nageswara Rao, T; Hansen, N; Hilfiker, J; Rai, S; Majewska, JM; Lekovic, D; Gezer, D; Andina, N; Galli, S; Cassel, T; Geier, F; Delezie, J; Nienhold, R; Hao-Shen, H; Beisel, C; Di Palma, S; Dimeloe, Sarah; Trebicka, J; Wolf, D; Gassmann, M

DOI:
10.1182/blood.2019000162

JAK2 mutant hematopoietic cells display metabolic alterations that can be targeted to treat myeloproliferative neoplasms

Tata Nageswara Rao[1*], Nils Hansen[1], Julian Hilfiker[1], Shivam Rai[1], Julia-Magdalena Majewska[1], Danijela Leković[2], Deniz Gezer[3], Nicola Andina[1], Serena Galli[1], Teresa Cassel[4], Florian Geier[1], Julien Delezie[5], Ronny Nienhold[1], Hui Hao-Shen[1], Christian Beisel[6], Serena Di Palma[7], Sarah Dimeloe[8], Jonel Trebicka[9], Dominik Wolf[10], Max Gassmann[11], Teresa W-M. Fan[4], Andrew N. Lane[4], Christoph Handschin[5], Stefan Dirnhofer[12], Nicolaus Kröger[13], Christoph Hess[8], Thomas Radimerski[14], Steffen Koschmieder[3], Vladan P. Čokić[15], and Radek C. Skoda[1*]

[1]Department of Biomedicine, Experimental Hematology, University Hospital Basel and University of Basel, 4031 Basel, Switzerland

[2]Clinic of Hematology, Clinical Center of Serbia, Belgrade, Serbia

[3]Department of Hematology, Oncology, Hemostaseology, and Stem Cell Transplantation, Faculty of Medicine, RWTH Aachen University, Aachen, Germany

[4]Center for Environmental and Systems Biochemistry, Department of Toxicology and Cancer Biology and Markey Cancer Center, University of Kentucky, KY 40536-0305 Kentucky, USA

[5]Biozentrum, University of Basel, Klingelbergstrasse 50/70, CH-4056 Basel, Switzerland

[6]Department of Biosystems Science and Engineering, ETH Zurich, Basel, Switzerland

[7]Functional Genomics Center Zurich, ETH Zurich/University of Zurich Winterthurerstr asse190, 8057 Zurich, Switzerland

[8]Immunobiology Laboratory, Department of Biomedicine, University Hospital Basel and University of Basel, Hebelstrasse 20, 4031 Basel, Switzerland, and Department of Medicine, University of Cambridge, Puddicombe Way, Cambridge CB2 0AW, UK

[9]Department of Internal Medicine I, University of Bonn, Bonn, Germany; European Foundation for the Study of Chronic Liver Failure - EF CLIF, Barcelona, Spain; Department of Gastroenterology, Odense Hospital, University of Southern Denmark, Odense, Denmark; Institute for Bioengineering of Catalonia, Barcelona, Spain

[10]Internal Medicine V, Department of Hematology and Oncology, Medical University Innsbruck, Innsbruck, Austria and Medical Clinic III for Oncology, Hematology, Immunoncology and Rheumatology, University Hospital Bonn (UKB), Bonn, Germany

[11]Institute of Veterinary Physiology, Vetsuisse Faculty and Zurich Center for Integrative Human Physiology, University of Zürich, Winterthurerstrasse 260, 8057 Zürich, Switzerland

[12]Institute of Pathology, University Hospital Basel, 4031 Basel, Switzerland [13]Department of Stem Cell Transplantation, University Hospital Eppendorf, Hamburg, Germany

[14]Disease Area Oncology, Novartis Institutes for Biomedical Research, Basel, Switzerland

[15]Institute for Medical Research, University of Belgrade, Belgrade, Serbia

Running title: Energy crisis in JAK2 mutant hematopoietic cells

Article type:	Regular Article
Scientific Category:	Myeloid Neoplasia
Word count:	Abstract: 223
	Text: 3997
Figure count:	7
Table count:	0
Supplements:	1 Supplemental Methods file, 8 Supplemental Figures, and 7 Supplemental Tables
Reference count:	44

Corresponding author: radek.skoda@unibas.ch or rao.tata@unibas.ch

Key Points

- Mutant *JAK2* induces a hitherto unrecognized metabolic phenotype, consisting of hypoglycemia, adipose tissue atrophy and early mortality
- Increased energy demands of *JAK2* mutant hematopoietic cells can be targeted by metabolic inhibitors to treat myeloproliferative neoplasms

Abstract

Increased energy requirement and metabolic reprograming are hallmarks of cancer cells. We show that metabolic alterations in hematopoietic cells are fundamental to the pathogenesis of mutant JAK2 driven myeloproliferative neoplasms (MPNs). We found that expression of mutant JAK2 augmented and subverted metabolic activity of MPN cells resulting in systemic metabolic changes in vivo, including hypoglycemia, adipose tissue atrophy and early mortality. Hypoglycemia in MPN mouse models correlated with hyperactive erythropoiesis and was due to a combination of elevated glycolysis and increased oxidative phosphorylation. Modulating nutrient supply through high fat diet improved survival, while high glucose diet augmented the MPN phenotype. Transcriptomic and metabolomic analyses identified numerous metabolic nodes in JAK2 mutant hematopoietic stem and progenitor cells that were altered in comparison with wildtype controls. We studied the consequences of elevated levels of Pfkfb3, a key regulatory enzyme of glycolysis, and found that pharmacological inhibition of Pfkfb3 with the small molecule 3PO reversed hypoglycemia and reduced hematopoietic manifestations of MPN. These effects were additive with the JAK1/2 inhibitor, Ruxolitinib, in vivo and in vitro. Inhibition of glycolysis by 3PO altered the redox homeostasis, leading to accumulation of reactive oxygen species and augmented apoptosis rate. Our findings reveal the contribution of metabolic alterations to the pathogenesis of MPN and suggest that metabolic dependencies of mutant cells represent vulnerabilities that can be targeted for treating MPN.

KEY WORDS

myeloproliferative neoplasms, JAK2, hypoglycemia, lipolysis, reactive oxygen species, redox homeostasis, Ruxolitinib.

INTRODUCTION

Myeloproliferative neoplasms (MPNs) are clonal disorders of hematopoietic stem cells (HSCs) driven by gain-of-function mutations in *JAK2, MPL* or *CALR* genes.[1-7] Additional mutations that modify the course of disease have also been described.[8] Three phenotypic manifestations of MPN can be distinguished: polycythemia vera (PV), essential thrombocythemia (ET) and primary myelofibrosis (PMF).[9]

Genetic and epigenetic changes associated with cancers are often coupled with reprogramming of cellular metabolism, a paradigm that has been recognized as one of the hallmarks of cancers.[10] Transformed cells require increased supply of nutrients to fuel their augmented energy demands and produce macromolecules needed for unconstrained proliferation and differentiation capacities.[11,12] Cancer cells can also reprogram metabolism of neighboring non-malignant cells through interactions with stromal cells and adipocytes by provoking them to secrete lipids, amino acids and other soluble factors, which can directly influence disease progression.[13,14] This may lead to cachexia, a life-threatening pathological condition with adipose tissue atrophy and muscle wasting. Indeed, survival of cancer patients is inversely correlated with the severity of cachexia.[15,16] Therefore, delineating differences in metabolic activities between normal and cancer cells is important and may open new therapeutic approaches.

We studied conditional transgenic mouse models of MPN that can be induced by tamoxifen to express either *JAK2*-V617F (*VF*),[17,18] or a *JAK2* exon 12 *(N542-E543del*) mutation (*E12*) in hematopoietic cells.[19] We have previously shown that these mouse models recapitulate the phenotypes of MPN patients including aberrant production of platelets and erythrocytes and the development of splenomegaly. These mice also show early mortality through incompletely understood mechanisms.[18,19]

Here we show that expression of mutant *JAK2* in hematopoietic cells leads to cell-autonomous metabolic alterations such as increase in glycolysis and oxidative phosphorylation, as well as to systemic changes, including hypoglycemia and adipose atrophy. We found that these JAK2 dependent metabolic alterations can be targeted therapeutically *in vivo* by limiting nutrient supply and by inhibiting rate-limiting steps in glycolysis with beneficial effects on MPN manifestations and survival.

METHODS

Mice used in this study were kept in accordance with Swiss federal regulations and all experiments were approved by the Cantonal Veterinary Office of Basel-Stadt. The collection of blood samples and clinical data from MPN patients was approved by the Ethik Kommission Beider Basel and the Ethics Boards of the University of Bonn and RWTH Aachen University, Germany and the Clinical Center of Serbia, University of Belgrade, Serbia. Written informed consent was obtained from all patients in accordance with the Declaration of Helsinki. The diagnosis of MPN was established according to the revised criteria of the World Health Organization.[9]

Data Sharing Statement

For detailed description of methods see supplement available with the online version of this article.

For original data and reagents, please contact radek.skoda@unibas.ch.

RNAseq data are available at GEO under accession number GSE 116571.

RESULTS

Adipose tissue atrophy and severe hypoglycemia in mice expressing *JAK2*-V617F or *JAK2* exon 12 mutant in hematopoietic cells

SclCre^{ER};JAK2-V617F (*VF*) and *SclCre^{ER};JAK2-N542-E543del* exon 12 mutant mice (*E12*), develop MPN within 4-5 weeks after induction with tamoxifen.[18,19] We noticed that these mice also displayed a marked reduction of fat tissues and a significant decrease in body weight that until now have gone unnoticed (Figure 1A and B). Epididymal white adipose tissue (eWAT) was dramatically reduced leading to an increase in lean body mass (Figure 1C and D), despite increased food intake and a trend towards reduced physical activity (Figure 1E and F). *VF* and *E12* strains both displayed hypoglycemia (Figure 1G). Serum insulin levels were not suppressed, possibly reflecting a hyperactive insulin axis (Figure 1H). After induction of the mutant *JAK2* by tamoxifen, hypoglycemia manifested earlier in *E12* mice than in *VF* mice (Figure 1I) and preceded the reduction in body weight (Figure 1J). Glucose tolerance test showed that exogenous glucose was immediately utilized in both *VF* and *E12* mice (Figure 1K). Ruxolitinib, a JAK1/2 tyrosine kinase inhibitor, normalized glucose levels in *E12* mice, along with a reduction of red cell parameters (Figure 1L). The metabolic changes were also present in mice transplanted with *VF* or *E12* bone marrow cells (Figure 1M), indicating that expression of mutant JAK2 solely in hematopoietic cells is sufficient to transfer the metabolic alterations.

To determine whether increased supply of glucose can correct the MPN associated hypoglycemia and influence disease manifestations, we exposed *JAK2* mutant mice and controls to high glucose diet (HGD). However, HGD was unable to correct hypoglycemia in *E12* mice (Figure 2A), while an increase in erythroid parameters in peripheral blood was noted in *VF* mice (Figure 2B) and an increase in spleen weight occurred in *E12* mice (Figure 2C). Thus, HGD did not ameliorate hypoglycemia, but rather fueled erythrocytosis and splenomegaly.

We next examined whether reducing glucose supply through intermittent fasting-feeding regimen may alter the disease course of MPN. Caloric restriction by intermittent fasting-feeding regimen was shown to affect hematopoietic stem and progenitor cell frequencies and their differentiation capacity also in wildtype mice.[20] Fasting-feeding regimen lowered blood glucose in *VF* recipients and in wildtype mice compared to uninterrupted feeding,

but glucose was uniformly very low in *E12* mice irrespective of regimen (Figure 2D). However, *E12* mice exposed to fasting-feeding displayed slightly lower red cell parameters and neutrophil numbers (Figure 2E) and also significantly reduced erythroid progenitors in bone marrow, while erythroid progenitors in spleen were increased (Supplemental Figure S1B). Spleen weight was markedly reduced in *E12* mice (Figure 2F). Thus, reducing glucose and energy supply through intermittent fasting ameliorated MPN phenotypes including splenomegaly and blood counts in *E12* mutant mice. The less prominent changes in *VF* mice are likely die to the slower kinetics of developing MPN after tamoxifen compared to the *E12* mice.

To assess whether elevated blood counts and increased hematopoietic activity correlates with hypoglycemia, we examined glucose levels in several additional knock-in or transgenic *JAK2*-V617F models of MPN that display various degrees of ET or PV phenotypes,[21-23] and in a transgenic line (*Tg6*) that constitutively overexpresses *erythropoietin* (*Epo*) and displays massive erythrocytosis.[24] A strong inverse correlation between blood glucose concentration and red cell parameters e.g. hemoglobin (R^2=0.822) was noted, whereas no correlation was seen between glucose and platelets, neutrophils or monocytes (Figure 2G). Hypoglycemia was present in all *JAK2*-V617F models with PV phenotype and also in *Tg6* mice with erythrocytosis, as previously reported.[25] However, hypoglycemia was absent in *JAK2*-V617F mice with a pure ET phenotype. These results suggest that increased glucose consumption by hyperactive erythropoiesis could be responsible for hypoglycemia in these mouse models.

To further examine glucose usage, we determined glucose uptake using the fluorescent tracer 2-NBDG. *VF* and *E12* cells showed increased glucose uptake compared to wildtype controls (Figure 2H and I). Interestingly, the intensity of 2-NBDG showed bi-modal peaks, possibly indicating that a subset of *VF* and *E12* cells is hyperactive in taking up glucose (Figure 2H). Erythroid cells of *E12* mice from spleen showed higher uptake than cells from bone marrow. Uptake of 2-NBDG in subsets of erythroid precursors was highest in the fractions II and III, correlating with the highest proliferative activity of these fractions (Figure 2I). Thus, erythroid cells in MPN mice take up and avidly consume glucose.

Since MPN mice showed severe loss of adipose deposits (Figure 1A-C), we tested whether high fat diet (HFD) may impact the MPN phenotype and survival. While wildtype mice on

HFD (60% fat) gained weight rapidly and after 24 weeks displayed a massive increase in body fat, *E12* mice showed little or no weight gain or increase in body fat (Figure 3A and B). Female *VF* mice failed to gain weight similar to *E12* mice, whereas male *VF* mice showed a moderate increase of weight. HFD increased leptin levels compared to normal chow, but the relative increase was greater in wildtype mice (Figure 3C). Hypoglycemia in VF and E12 mice was not corrected by HFD, although a trend towards slightly higher levels was noted (Figure 3D). Insulin levels increased under HFD in *VF* despite hypoglycemia, but remained unchanged in *E12* mice (Figure 3E). Remarkably, survival of *E12* mice was substantially prolonged by HFD ($p<0.001$) and allowed us to follow these mice for up to 30 weeks (Figure 3F). There was only a trend towards better survival in *VF* mice. HFD treatment has been shown to negatively impact hematopoietic differentiation capacity of HSPCs in the BM niche.[26] We observed slightly reduced red cell parameters, but increased spleen size in JAK2 mutant mice on HFD (Figure 3G and H).

On normal chow, adipocytes from *VF* and *E12* mice showed significantly reduced size compared to wildtype (Figure 3I). On HFD, the size of adipocytes increased in all genotypes, but adipocytes from *VF* and *E12* mice remained smaller than adipocytes from wildtype mice (Figure 3G). Fat tissue from *VF* and *E12* mice also displayed elevated mRNA expression of several inflammatory cytokines as well as *CD36,* a fatty acid uptake mediator (Supplemental Figure S2A). Mutant *JAK2* also altered brown adipose tissue (BAT) morphology, with increased numbers of small fat vacuoles. HFD partially normalized these alterations (Supplemental Figure S2B). In line with the elevated lipolysis, HFD treated *VF* and *E12* mice displayed reduced accumulation of lipids in the liver (Supplemental Figure S2C), suggesting that these mice are less prone to hepatic steatosis upon an HFD challenge.

Our data suggest that hematopoietic specific expression of mutant *JAK2* induces hypoglycemia due to increased consumption of glucose by erythroid cells, which was normalized by Ruxolitinib, and increased energy demand and elevated inflammatory cytokines lead to lipolysis and adipose atrophy that was partially corrected by HFD.

Since some of the metabolic alterations, in particular lipolysis, appears to be a counter-regulatory adaptation to hypoglycemia involving non-hematopoietic tissues, we next sought to specific metabolic requirements that are unique to *JAK2* mutant hematopoietic

progenitor and stem cells (HSPCs). We performed RNA sequencing in megakaryocyte and erythroid progenitors (MEPs) of *JAK2* mutant and wildtype mice. The numbers of differentially expressed genes in MEPs from bone marrow of *VF* and *E12* mice compared to wildtype MEPs and the heatmaps are shown in Figure 4A and B. Ingenuity Pathway Analysis based Gene Ontology enrichment revealed that most of the significantly up/down regulated genes in *JAK2* mutant mice were related to metabolism, JAK/STAT signaling and inflammatory signaling pathways (Supplemental Figure S3A). By competitive gene set testing on the MSigDB hallmark gene sets,[27] we also found that oxidative phosphorylation and JAK/STAT signaling target genes were among the four top gene sets (Supplemental Figure S3B). Consistent with the elevated glucose uptake (Figure 2E and F), we observed increased expression of glucose transporters (*Glut1, Glut3,* and *Glut10*), of glutamine transporter *Asct2,* and the *Slc27a* family of fatty acid transporters (Figure 4C). Furthermore, enzymes involved in regulation of glycolysis (e.g. *Pkm1 and Pfkfb3)* and their known transcriptional regulators (e.g. *Hif-1α, nMyc, Ahr* and *Arnt)* were also elevated in MEPs from *VF* and *E12* mice (Figure 4D and E). These data suggest that activation of mutant JAK2 signaling alters the expression of genes involved the regulation of metabolic pathways.

Analysis of mRNA expression was complemented with profiling of metabolite in purified bone marrow MEP cells using liquid chromatography coupled to mass spectrometry. We found altered concentrations of metabolites that were classified into groups using Metabolic Pathway Enrichment Analysis (Figure 4F).[28] The observed changes in *JAK2* mutant MEPs were consistent with increased activities of glycolysis, pentose phosphate pathway and terpenoid backbones for steroid biosynthesis (Figure 4F) and the same changes were also observed in lineage-negative, Sca-1^+ and cKit^+ (LSK) cells (Supplemental Figure S4A). Combined analysis of data obtained by RNA sequencing and metabolite profiling also showed altered regulation of glycolysis and pentose phosphate pathway genes as the main alterations in MEPs from *JAK2* mutant mice (Supplemental Figure S4B).

To assess glycolytic activity and mitochondrial respiration, we performed metabolic flux studies. Aerobic glycolysis, indicative of Warburg effect,[11,29] was elevated in LSK and MEP cells from *VF* and *E12* mice (Figure 4G). The same results were obtained in total spleen cells (Supplemental Figure S4C). However, total bone marrow cells from *E12* mice

unexpectedly showed slightly reduced rate of glycolysis compared to wildtype bone marrow. Mitochondrial respiration was assessed by determining the oxygen consumption rate (OCR) as an indicator of oxidative phosphorylation. Bone marrow LSK and MEP cells from *VF* and *E12* mice showed an increased respiration rate compared with wildtype controls (Figure 4H). Likewise, unfractionated spleen cells from *VF* and *E12* mice also showed increased basal respiration rate and a higher maximal respiration rate than wildtype controls (Supplemental Figure S4D). No differences in OCR between total bone marrow cells from *VF*, *E12* and wildtype mice were detected (Supplemental Figure S4D). In line with the increased rate of glycolysis and oxidative phosphorylation, LSK and MEPs from *VF* and *E12* mice showed increased glucose uptake (Figure 4I), similar to differentiated erythroid cells (Figure 2H and I).

Since mitochondrial respiration was increased, we used several methods to determine mitochondrial numbers and mass. Transmission electron microscopy (TEM) showed that LSK and MEP cells of *VF* mice had reduced numbers of mitochondria, while the number of mitochondria of *E12* mice were increased in MEPs (Figure 4J). Likewise, quantification of mitochondrial DNA copy number by qPCR in *E12* showed a similar pattern of decrease in LT-HSCs and increase in MEPs (Figure 4K), while in *VF* mice no differences were noted to wildtype mice. A similar pattern was observed using the mitochondrial membrane specific dye MitoTracker Green (Supplemental Figure S4E). These results show an overall trend towards a decrease in mitochondrial numbers and mitochondrial mass in cells from *JAK2* mutant mice. Thus, despite reduced mitochondrial mass, HSPCs from *JAK2* mutant mice showed an increased rate of oxidative phosphorylation. We found decreased mitochondrial DNA copy number also in peripheral blood granulocytes from MPN patients (Figure 4L).

Since hematopoietic cells of *JAK2* mutant mice showed elevated expression of glucose transporters and increased glucose uptake, we examined in more detail the intracellular fate of glucose by tracking ^{13}C-labeled D-glucose ([U-$^{13}C_6$] D-glucose) (Figure 5A). Purified MEP and LSK cells were cultured for 8 hours in serum free medium with [U-$^{13}C_6$] D-glucose and the total abundance of metabolites as well as the abundance of ^{13}C-labeled metabolites was determined by ion chromatography–Fourier transform mass spectrometry.[30] The glycolytic intermediates showed a high percentage ^{13}C labeling in both WT and *JAK2* mutated cells, while the absolute amounts of glycolytic intermediates were

elevated only in cells from *JAK2* mutant mice (Figure 5B), consistent with increased rate of glycolysis. The total amount of pyruvate in *JAK2* mutant cells was higher than that of WT cells, in good correlation with the increased expression of *pyruvate kinase* (*Pkm1*). However, only 20-30% of pyruvate was labeled with ^{13}C in cells from all genotypes, suggesting that a major proportion of pyruvate came from non-glucose sources, e.g. amino acid metabolism. Consequently, the percentage of contribution of the ^{13}C labeled pyruvate to the TCA cycle was low (Supplemental Figure S5A). Cells expressing mutant *JAK2* also showed strong ^{13}C labeling of pentose phosphate pathway (PPP) intermediates, leading to increased biosynthesis of purine nucleotides (Figure 5B and Supplemental Figure S5B). Consistently, *phosphoribosyl pyrophosphate synthetase 2 (Prps2*), the rate-limiting enzyme for PRPP synthesis, was highly elevated in *JAK2* mutant HSPCs (Supplemental Figure S5C).

Taken together, these data suggest that expression of mutant *JAK2* in hematopoietic cells reprograms metabolism by upregulating the expression of nutrient transporters and key regulatory enzymes of glucose metabolism resulting in increased glycolysis, mitochondrial respirations and nucleotide biosynthesis.

Targeting the activity of Pfkfb3, an early rate-limiting enzyme in glycolysis reduces growth of human *JAK2*-V617F expressing cell lines

We found that *Pfkfb3,* one of four Pfkfb isoforms, was significantly elevated in mutant HSPCs both on RNA and protein levels (Figure 5C and D). This enzyme catalyzes the conversion of fructose-6-phosphate (F6P) to fructose-2,6-bisphosphate (F2,6BP), which acts as an allosteric activator on phosphofructokinase (Pfk1) and thereby accelerates one of the rate-limiting steps in glycolysis (Figure 5E).[31] Pfkfb3 can be inhibited by 3PO (3-(3-pyridinyl)-1-(4-pyridinyl)-2-propen-1-one),[32] a small molecule that was found to reduce the intracellular concentration of F2,6BP and thereby to suppresses glycolysis.[31] We first tested 3PO alone or in combination with Ruxolitinib on growth, survival, and metabolic activity in human myeloid cell lines SET2, HEL and UKE1 that express *JAK2*-V617F, and in K562 cells that are transformed by BCR-ABL. We confirmed that the *PFKFB3* was expressed in these cells (Supplemental Figure S6A). Treatment with 3PO alone increased apoptosis and attenuated the proliferation of all *JAK2*-V617F expressing cell lines in a dose dependent manner and this effect was additive with Ruxolitinib (Figure 6A and B and Supplemental Figure S6B). In contrast, K562 cells were susceptible to 3PO treatment only

at high concentrations (Figure 6A and B). *JAK2*-V617F expressing cell lines treated with 3PO alone for 12 hours showed markedly reduced glycolytic rate in a dose-dependent manner and exhibited additive effects with Ruxolitinib (Figure 6C). Interestingly, 3PO also reduced mitochondrial oxygen consumption rate (Figure 6D), possibly due to reduced supply of glycolysis pathway intermediates to the TCA cycle. Under similar conditions, no effect of 3PO on glycolysis or oxygen consumption was observed in K562 cells. These results suggest that human cell lines expressing *JAK2*-V617F highly depend on glycolysis and are susceptible to apoptotic cell death when subjected to glycolytic blockade.

Perturbation of glycolysis and mitochondrial respiration can lead to altered redox homeostasis and aberrant levels of reactive oxygen species (ROS). 3PO alone caused an increase in total ROS levels already at 6 hours after treatment (Supplemental Figure S6C). Elevated ROS levels in SET2 cells persisted for at least 24 hours (Figure 6E) and resulted in increased apoptosis and decreased proliferation (Figure 6F and G). This suggested that the blockade of glycolysis by 3PO in *JAK2*-V617F expressing cells rapidly depleted the cellular antioxidant capacities. Indeed, treatment with 3PO alone or in combination with Ruxolitinib reduced the ratio of glutathione (GSH) to glutathione disulfide (GSSG, the oxidized form of GSH) (Figure 6H). Consistent with diminished GSH/GSSG ratios, 3PO treatment alone or in combination with Ruxolitinib also substantially reduced NADPH levels (Figure 6I), suggesting that decreased flux through the pentose phosphate pathway contributed to exhaustion of reductive reserves and defects in redox homeostasis in *JAK2*-V617F cells. The functional consequences of ROS-mediated actions are highly dose dependent: moderate increases in ROS may potentiate cell survival and proliferation, whereas high ROS levels that exceed cellular antioxidant capacity are detrimental to cell survival.[33,34] The depleted antioxidant capacities of GSH or NADPH could be partially rescued by N-Acetyl-L-Cysteine (NAC), a potent ROS scavenger (Figure 6H and I).[13] NAC treatment in SET2 cells not only lowered ROS levels close to baseline (Figure 6e), but also rescued OCR (Supplemental Figure S6D) as well as cell survival and proliferation disadvantage caused by 3PO (Figure 6E-H). 3PO treatment also caused apoptosis of peripheral blood mononuclear cells from MPN patients with high JAK2-V617F allele burden, which was rescued by NAC pre-treatment (Supplemental Figure S7). These data suggested that inhibition of glycolysis through 3PO increased ROS levels above the cellular antioxidant capacity and thereby contributes to inhibiting proliferation and survival of *JAK2*-V617F expressing cells.

We then assessed the efficacy and tolerability of 3PO treatment in vivo in a cohort of *VF* or *E12* mice. To allow monitoring of mutant JAK2 allele burden, competitive transplantation of bone marrow co-expressing mutant JAK2 with a GFP-reporter and wildtype mice in a 1:1 mixture were performed (Figure 7A). Recipient mice treated with 3PO alone or in combination with Ruxolitinib for 8 weeks showed reduction of spleen weight, increase in eWAT, and improved glucose levels including normalization of glucose tolerance (Figure 7B-E). 3PO also restored body fat in *JAK2* mutant mice (Supplemental Figure S8A) and combination with Ruxolitinib augmented these beneficial effects (Figure 7B-E). Consistently, MPN patients significantly gained body weight when treated with Ruxolitinib (Supplemental Figure S8B), in line with previous reports.[35,36] In *VF* mice, 3PO treatment alone also reduced red cell numbers, hemoglobin levels, and neutrophils (Figure 7F). These reductions were accentuated in combination of 3PO with Ruxolitinib. 3PO alone had no effect on platelet counts, while Ruxolitinib alone or in combination with 3PO increased platelet numbers in *VF* and *E12* mice. This paradoxical effect of Ruxolitinib on platelets has been reported previously.[18,37] Our data obtained in human hematopoietic cell lines expressing JAK2-V617F and primary samples from MPN patients suggest that the same metabolic alterations as in mouse models are present in human MPN. Furthermore, PV patients under cytoreductive therapies showed higher glucose levels (95.3 ± 13.5) as compared to PV patients on phlebotomy only (81.8 ± 6.1) (Figure 7G). Taken together, these data suggest that targeting metabolic alterations in MPN may open new therapeutic opportunities also for human MPN.

DISCUSSION

We show that expression of mutant *JAK2* in mouse models of MPN induces profound metabolic alterations that have been hitherto overlooked, with strongly increased energy demands and vital dependence on glucose. In mouse models of AML, leukemic cells expressing both BCR/ABL and NUP98/HOXA9, or MLL-AF9 alone imposed systemic metabolic changes resulting in mild hypoglycemia with markedly decreased insulin levels and insulin resistance.[38] In contrast, our mutant *JAK2* models displayed a more profound hypoglycemia without signs of insulin resistance, implying that AML and MPN cells differ in the type and extent of the metabolic reprograming. Hypoglycemia strongly correlated with the degree of increased erythropoiesis, consistent with the critical role of glucose metabolism in normal erythropoiesis.[39] *E12* mice, with predominantly erythroid hyperproliferation, had a more severe hypoglycemia than *VF* mice that display tri-lineage involvement and a milder erythroid phenotype. Hypoglycemia was also observed in *Tg6* mice that exhibit massive erythrocytosis due to transgenic overexpression of *Epo* under the control of the human *PDGFR* promoter.[24,25] This suggests that excessive Epo signaling through wildtype JAK2 can lead to similar metabolic alterations as signaling through mutant JAK2.

In addition to altered glucose metabolism, *JAK2* mutant mice also exhibited increased lipid catabolism. The changes in lipid metabolism could be a consequence of the general energy crisis induced by hypoglycemia, but chronic inflammation mediated by elevated cytokine production may further contribute to lipolysis in a non-cell autonomous way. Cachexia in advanced PMF was also linked to increased levels of pro-inflammatory cytokines.[40] *Tg6* mice also showed decreased fat stores,[25] supporting a connection between excess erythropoiesis and lipolysis. However, *Tg6* mice typically survive for 28-32 weeks,[41] whereas *E12* mice die within 8-10 weeks. Thus, signaling through mutant JAK2 has more deleterious consequences than signaling through wildtype JAK2 due to overexpressing of Epo.

Metabolic phenotyping and gene expression analyses of HSPCs revealed profound alterations in multiple metabolic pathways and allowed us to identify several potentially rate-limiting steps in glycolysis, pentose phosphate cycle and citrate cycle. Inhibiting glycolysis by 3PO in *JAK2*-V617F expressing human cell lines reduced proliferation and

increased apoptosis through a mechanism that involves greatly increased ROS levels (Figure 6). Although the extent of metabolic alterations in patients with MPN remains to be determined, the effectiveness of 3PO inhibition in *JAK2* mutant human cell lines and primary samples from MPN patients is encouraging. 3PO also reduced blood counts and spleen size and normalized glucose levels and fat tissues in *JAK2* mutant mice *in vivo*, further suggesting that lipolysis is primarily driven by increased glucose consumption and energy crisis (Figure 7H). Poor water solubility of 3PO makes this compound difficult to administer in patients. However, derivatives of 3PO, such as PFK15 and PFK-158 that also inhibit PFKFB3 are now in clinical trials for treating late-stage cancer patients.[42]

Increased glutamine metabolism was reported in BaF/3 cells expressing JAK2-V617F mutation.[43] It will be interesting to determine whether targeting glutamine metabolism alone or in combination with inhibition of glycolysis can improve the therapy of MPN. A recent study investigated the cell-autonomous metabolic changes in mutant IDH2/JAK2 driven MPN (present in 2% of MPN patients) and demonstrated that JAK2/IDH-mutant cells are sensitive to an IDH2 inhibitor.[44] While the presence of additional somatic mutation in MPN may be difficult to target therapeutically, the resultant metabolic abnormalities might be common for different driver mutations and could represent new therapeutic targets.

Our findings underpin the potential of elucidating additional MPN cell specific metabolic properties and provide a rationale for testing metabolic inhibitors in MPN using a “two-pronged” approach of co-targeting altered metabolic dependencies and mutant JAK2 activity.

ACKNOWLEDGMENTS

We thank members of the laboratory members for helpful discussions and critical reading of our manuscript, Dr. Jean-Luc Villeval and Dr. Anthony R. Green for providing the mouse *Jak2*-V617F knockin and human *JAK2*-V617F knockin mice, respectively, and Philippe Demougin and Katja Eschbach (D-BSSE, Genomics Facility Basel) for conducting next-generation sequencing. The analyses of RNASeq data were performed at sciCORE (http://scicore.unibas.ch/) scientific computing center at University of Basel. Dr. Endre Laczko (Functional Genomics Center Zürich) for helpful discussions on metabolomics analysis. Petra Seebeck (University of Zurich) for performing EchoMRI scans of mice. This work was supported by grants from the Swiss National Science Foundation (31003A-147016/1 and 31003A_166613), SystemsX.ch (Medical Research and Development grant 2014/266), and the Swiss Cancer League (KLS-2950-02-2012 and KFS-3655-02-2015) to RCS, and by a grant from the Forschungsfonds der Universität Basel (DMM 2039) and Krebsliga Beider Basel (KLbB-4486) to TNR. Stable isotope resolved metabolomics was performed with the support of the Resource Facility for Stable Isotope Resolved Metabolomics funded by NIH grant # 1U24DK097215-01A1 to TWMF.

AUTHOR CONTRIBUTIONS

TNR designed and performed research, analyzed data and wrote the manuscript, NH, JH, SR, JM, NA, SG, DL, DG, RN, TC, ANL, TWF, CB, SK, VPC, and SDP performed research and analyzed data, FG analyzed data, HH performed mice genotyping. JT, DW, and NK collected and analyzed MPN patient data, JD and CH performed research and analyzed data, SD performed research and analyzed data, SD, CH and TR analyzed data, RCS designed research, analyzed data and wrote the manuscript.

Conflict-of-interest disclosure:

T.R. is a full-time employee of Novartis Pharma AG, R.C.S. has consulted for and received honoraria from Novarts, Shire and Baxalta, S.K. reports research funding from Novartis, AOP Orphan Pharmaceuticals AG, and Bristol-Myers Squibb as well as consultancy honoraria and travel reimbursements from Novartis, AOP Orphan Pharmaceuticals AG, and Bristol-Myers Squibb. The other authors declare no competing financial interests.

REFERENCES

1. Kralovics R, Passamonti F, Buser AS, et al. A gain-of-function mutation of JAK2 in myeloproliferative disorders. *N Engl J Med*. 2005;352(17):1779-1790.
2. Levine RL, Wadleigh M, Cools J, et al. Activating mutation in the tyrosine kinase JAK2 in polycythemia vera, essential thrombocythemia, and myeloid metaplasia with myelofibrosis. *Cancer Cell*. 2005;7(4):387-397.
3. James C, Ugo V, Le Couedic JP, et al. A unique clonal JAK2 mutation leading to constitutive signalling causes polycythaemia vera. *Nature*. 2005;434(7037):1144-1148.
4. Baxter EJ, Scott LM, Campbell PJ, et al. Acquired mutation of the tyrosine kinase JAK2 in human myeloproliferative disorders. *Lancet*. 2005;365(9464):1054-1061.
5. Klampfl T, Gisslinger H, Harutyunyan AS, et al. Somatic mutations of calreticulin in myeloproliferative neoplasms. *N Engl J Med*. 2013;369(25):2379-2390.
6. Nangalia J, Massie CE, Baxter EJ, et al. Somatic CALR mutations in myeloproliferative neoplasms with nonmutated JAK2. *N Engl J Med*. 2013;369(25):2391-2405.
7. Pikman Y, Lee BH, Mercher T, et al. MPLW515L is a novel somatic activating mutation in myelofibrosis with myeloid metaplasia. *PLoS Med*. 2006;3(7):e270.
8. Vainchenker W, Kralovics R. Genetic basis and molecular pathophysiology of classical myeloproliferative neoplasms. *Blood*. 2017;129(6):667-679.
9. Arber DA, Orazi A, Hasserjian R, et al. The 2016 revision to the World Health Organization classification of myeloid neoplasms and acute leukemia. *Blood*. 2016;127(20):2391-2405.
10. Hanahan D, Weinberg RA. Hallmarks of cancer: the next generation. *Cell*. 2011;144(5):646-674.
11. Vander Heiden MG, Cantley LC, Thompson CB. Understanding the Warburg effect: the metabolic requirements of cell proliferation. *Science*. 2009;324(5930):1029-1033.
12. Pavlova NN, Thompson CB. The Emerging Hallmarks of Cancer Metabolism. *Cell Metab*. 2016;23(1):27-47.
13. DeBerardinis RJ, Lum JJ, Hatzivassiliou G, Thompson CB. The biology of cancer: metabolic reprogramming fuels cell growth and proliferation. *Cell Metab*. 2008;7(1):11-20.
14. Ye H, Adane B, Khan N, et al. Leukemic Stem Cells Evade Chemotherapy by Metabolic Adaptation to an Adipose Tissue Niche. *Cell Stem Cell*. 2016;19(1):23-37.
15. Deans C, Wigmore SJ. Systemic inflammation, cachexia and prognosis in patients with cancer. *Curr Opin Clin Nutr Metab Care*. 2005;8(3):265-269.
16. Fearon K, Arends J, Baracos V. Understanding the mechanisms and treatment options in cancer cachexia. *Nat Rev Clin Oncol*. 2013;10(2):90-99.
17. Tiedt R, Hao-Shen H, Sobas MA, et al. Ratio of mutant JAK2-V617F to wild-type Jak2 determines the MPD phenotypes in transgenic mice. *Blood*. 2008;111(8):3931-3940.
18. Kubovcakova L, Lundberg P, Grisouard J, et al. Differential effects of hydroxyurea and INC424 on mutant allele burden and myeloproliferative phenotype in a JAK2-V617F polycythemia vera mouse model. *Blood*. 2013;121(7):1188-1199.
19. Grisouard J, Li S, Kubovcakova L, et al. JAK2 exon 12 mutant mice display isolated erythrocytosis and changes in iron metabolism favoring increased erythropoiesis. *Blood*. 2016;128(6):839-851.
20. Cheng CW, Adams GB, Perin L, et al. Prolonged Fasting Reduces IGF-1/PKA to Promote Hematopoietic-Stem-Cell-Based Regeneration and Reverse Immunosuppression. *Cell Stem Cell*. 2014;14(6):810-823.

21. Hasan S, Lacout C, Marty C, et al. JAK2V617F expression in mice amplifies early hematopoietic cells and gives them a competitive advantage that is hampered by IFNalpha. *Blood*. 2013;122(8):1464-1477.
22. Li J, Spensberger D, Ahn JS, et al. JAK2 V617F impairs hematopoietic stem cell function in a conditional knock-in mouse model of JAK2 V617F-positive essential thrombocythemia. *Blood*. 2010;116(9):1528-1538.
23. Li J, Kent DG, Godfrey AL, et al. JAK2V617F homozygosity drives a phenotypic switch in myeloproliferative neoplasms, but is insufficient to sustain disease. *Blood*. 2014;123(20):3139-3151.
24. Ruschitzka FT, Wenger RH, Stallmach T, et al. Nitric oxide prevents cardiovascular disease and determines survival in polyglobulic mice overexpressing erythropoietin. *Proc Natl Acad Sci U S A*. 2000;97(21):11609-11613.
25. Katz O, Stuible M, Golishevski N, et al. Erythropoietin treatment leads to reduced blood glucose levels and body mass: insights from murine models. *J Endocrinol*. 2010;205(1):87-95.
26. Naveiras O, Nardi V, Wenzel PL, Hauschka PV, Fahey F, Daley GQ. Bone-marrow adipocytes as negative regulators of the haematopoietic microenvironment. *Nature*. 2009;460(7252):259-263.
27. Liberzon A, Birger C, Thorvaldsdottir H, Ghandi M, Mesirov JP, Tamayo P. The Molecular Signatures Database (MSigDB) hallmark gene set collection. *Cell Syst*. 2015;1(6):417-425.
28. Xia J, Wishart DS. Using MetaboAnalyst 3.0 for Comprehensive Metabolomics Data Analysis. *Curr Protoc Bioinformatics*. 2016;55:14 10 11-14 10 91.
29. Warburg O. On the origin of cancer cells. *Science*. 1956;123(3191):309-314.
30. Fan TW, Warmoes MO, Sun Q, et al. Distinctly perturbed metabolic networks underlie differential tumor tissue damages induced by immune modulator beta-glucan in a two-case ex vivo non-small-cell lung cancer study. *Cold Spring Harb Mol Case Stud*. 2016;2(4):a000893.
31. Clem B, Telang S, Clem A, et al. Small-molecule inhibition of 6-phosphofructo-2-kinase activity suppresses glycolytic flux and tumor growth. *Mol Cancer Ther*. 2008;7(1):110-120.
32. Schoors S, De Bock K, Cantelmo AR, et al. Partial and transient reduction of glycolysis by PFKFB3 blockade reduces pathological angiogenesis. *Cell Metab*. 2014;19(1):37-48.
33. Perry G, Raina AK, Nunomura A, Wataya T, Sayre LM, Smith MA. How important is oxidative damage? Lessons from Alzheimer's disease. *Free Radic Biol Med*. 2000;28(5):831-834.
34. Ito K, Suda T. Metabolic requirements for the maintenance of self-renewing stem cells. *Nat Rev Mol Cell Biol*. 2014;15(4):243-256.
35. Harrison C, Kiladjian JJ, Al-Ali HK, et al. JAK inhibition with ruxolitinib versus best available therapy for myelofibrosis. *N Engl J Med*. 2012;366(9):787-798.
36. Verstovsek S, Mesa RA, Gotlib J, et al. A double-blind, placebo-controlled trial of ruxolitinib for myelofibrosis. *N Engl J Med*. 2012;366(9):799-807.
37. Besancenot R, Roos-Weil D, Tonetti C, et al. JAK2 and MPL protein levels determine TPO-induced megakaryocyte proliferation vs differentiation. *Blood*. 2014;124(13):2104-2115.
38. Ye HB, Adane B, Khan N, et al. Subversion of Systemic Glucose Metabolism as a Mechanism to Support the Growth of Leukemia Cells. *Cancer Cell*. 2018;34(4):659-+.
39. Oburoglu L, Tardito S, Fritz V, et al. Glucose and glutamine metabolism regulate human hematopoietic stem cell lineage specification. *Cell Stem Cell*. 2014;15(2):169-184.

40. Verstovsek S, Kantarjian H, Mesa RA, et al. Safety and efficacy of INCB018424, a JAK1 and JAK2 inhibitor, in myelofibrosis. *The New England journal of medicine*. 2010;363(12):1117-1127.
41. Wagner KF, Katschinski DM, Hasegawa J, et al. Chronic inborn erythrocytosis leads to cardiac dysfunction and premature death in mice overexpressing erythropoietin. *Blood*. 2001;97(2):536-542.
42. Mondal S, Roy D, Sarkar Bhattacharya S, et al. Therapeutic targeting of PFKFB3 with a novel glycolytic inhibitor PFK158 promotes lipophagy and chemosensitivity in gynecologic cancers. *Int J Cancer*. 2019;144(1):178-189.
43. Zhan HC, Ciano K, Dong K, Zucker S. Targeting glutamine metabolism in myeloproliferative neoplasms. *Blood Cells Molecules and Diseases*. 2015;55(3):241-247.
44. McKenney AS, Lau AN, Somasundara AVH, et al. JAK2/IDH-mutant-driven myeloproliferative neoplasm is sensitive to combined targeted inhibition (vol 128, pg 789 2018). *Journal of Clinical Investigation*. 2018;128(10):4743-4743.

FIGURE LEGENDS

Figure 1. Hematopoietic specific expression of mutant *JAK2* induced adipose tissue atrophy, severe hypoglycemia and global metabolic changes in MPN mice. (A) Representative pictures of wildtype (*WT*), *JAK2*-V617F *(VF)* and *JAK2;E12* (*E12*) mutant mice at 2-4 month after induction with tamoxifen. Red and blue asterisks indicate reduced subcutaneous and epididymal white adipose tissue (eWAT), respectively. (B) Body weight at 2-4 month after induction with tamoxifen (n= 8-12 mice per genotype). (C) Epididymal white adipose tissue weight (n= 8-12 mice per genotype). (D) Ratios of lean body mass to total body mass (solid colors) and ratio of fat mass to total body mass (transparent colors) at 2-4 month after induction with tamoxifen (n= 4-5 mice per group). (E and F) Food intake (E) and locomotor activity (on x-y-z axis) (F) as measured by comprehensive laboratory animal monitoring system (n=5 mice per genotype). (G) Non-fasting blood glucose levels at 12 weeks (*VF*) and 6 weeks (*E12*) after tamoxifen induction (n=5-6 mice per genotype). (H) Serum insulin levels at 12 weeks (*VF*) and 6 weeks (*E12*) after tamoxifen induction (n=5-6 mice per genotype) (n= 8 mice per genotype). (I and J) non-fasting blood glucose levels (I) and time course of change in body weight (J) after tamoxifen induction (n=5 mice per genotype). (K) Glucose tolerance test (GTT) 6 hours after starvation at 12 weeks (*VF*) and 6 weeks (*E12*) after tamoxifen induction (n= 10-12 mice per genotype). (L) Tamoxifen induced mice were treated with Ruxolitinib (90mg/kg, daily twice). Time course of fasting blood glucose levels, peripheral hemoglobin levels and reticulocyte counts (n= 5-6 mice per genotype). (M) GTT in recipients transplanted with bone marrow cells ($2x10^6$) from *WT, VF or E12* donor mice (n=6 mice per genotype). All data are presented as mean ± SEM. One-way or two-way ANOVA analyses followed by Tukey's multiple comparison tests were used for multiple group comparisons. *P < .05; **P < .01; ***P < .001.

Figure 2. Mutant *JAK2* induced MPN is vulnerable to modulation of nutrients *in vivo*. (A) Mice were induced by tamoxifen and treated with normal diet (ND) or HGD for 7 weeks. Time course of non-fasting blood glucose levels (n=5-6 mice per treatment and genotype). (B) Peripheral blood counts of HGD and ND treated mice (n=5-6 mice per genotype). (C) Spleen weight after 7 weeks of ND or HGD (n=5-6 mice per treatment and genotype). (D) Non-fasting blood glucose levels in mice exposed to fed-fasting cycles or continuously fed with normal diet (n=4-5 mice per genotype and condition). (E) Peripheral

blood counts of mice exposed to fed-fasting cycles or continuously fed with normal diet. (F) Spleen weight in mice exposed to fed-fasting cycles or normal diet (n=4-5 mice per genotype and condition). (G**)** Correlation of non-fasting blood glucose levels with the peripheral blood counts. Six to eight weeks after tamoxifen injections peripheral blood counts and non-fasting blood glucose levels were monitored (n=4-5 mice per genotype). (H and I) Glucose uptake capacity of erythroid cells in spleen monitored by 2-NBDG fluorescence. After 4 hours starvation, cells from spleen or bone marrow were exposed to 2-NBDG for 30 minutes and analyzed by flow cytometry. (H) Histograms show 2-NBDG fluorescence in splenic $CD71^{+}Ter119^{+}$ cells with quantification of the mean fluorescence intensity (MFI) presented as bar graphs (middle panel). Right panel shows 2-NBDG MFI in subsets of erythroid cells (I-V). (I) Glucose uptake capacity of erythroid cells in bone marrow (n=6 mice per genotype). All data are presented as mean ± SEM. One-way or two-way ANOVA analyses followed by Tukey's multiple comparison tests were used for multiple group comparisons. *P < .05; **P < .01.

Figure 3. High fat diet treatment ameliorated early lethality phenotype of polycythemia vera exhibiting mutant *JAK2* expressing mice. (A) Pictures of male wildtype (*WT)*, *VF* and *E12* mutant mice exposed to high fat diet (HFD) for 24 weeks. Red and blue asterisks mark reduced subcutaneous and epididymal white adipose tissue (eWAT) fat content, respectively. (B) Time course of body weight gain of HFD treated mice (n= 8-12 mice per genotype and gender). (C) Plasma leptin concentration in HFD and normal diet (ND) treated mice (n=5 mice per treatment and genotype). (D**)** Non-fasting blood glucose levels HFD or ND treated mice (n=5 mice per treatment and genotype). (E) Serum insulin levels in ND and HFD treated mice (n= 4-5 mice per treatment and genotype). (F**)** Survival of mice on ND or HFD (n=12 mice per treatment and genotype). (G**)** Hemoglobin levels, RBC, platelet and neutrophils counts in peripheral blood during HFD or ND treatment in indicated mice (n=6-8 mice per treatment and genotype). (H) Bar graph indicating spleen weight of HFD and ND treated mice (n=5-6 mice per genotype). (I) Representative images of hematoxylin and eosin (H&E) staining of eWAT from ND or HFD treated mice. Scale bars=100µm. Bar graph represents the median white adipocyte size of HFD treated mice (n=5 mice per). All data are presented as mean ± SEM. One-way or two-way ANOVA analyses followed by Tukey's multiple comparison tests were used for multiple group comparisons. Significance in survival curves was estimated with the log-rank test. *P ≤ .05; **P ≤ .01; ***P ≤ .001.

Figure 4. Transcriptomic and metabolic profiling identified altered metabolic pathways in hematopoietic stem and progenitor cells expressing mutant *JAK2.* (A) Venn diagram shows number of distinct and overlapping genes expressed between *VF* and *E12* mice as compared to wildtype (WT) controls (logFC>1.5 and FDR<0.05, n=3 per genotype). (B) Heat map showing differentially expressed genes in bone marrow MEPs as determined by mRNA sequencing. Data shows fold change to the mean. (C-E) Heat map showing expression of nutrient transporters (C), glycolysis pathway enzymes (D) and regulators of glycolysis pathway genes (E) in bone marrow MEPs as determined by mRNA sequencing. Data shown is normalized expression levels in *VF* and *E12* versus wildtype cells (n=3 per genotype). (F) Metabolic Pathway Enrichment Analysis of significantly up-regulated metabolites in bone marrow MEPs from *VF* and *E12* compared to wildtype mice as determined by MetaboloAnalyst 3.0 (n=3 per genotype; >1.5 fold-change; p<0.05). (G) Measurements of glycolytic rates in bone marrow LSK and MEPs. Extracellular acidification rate (ECAR) values were normalized to cell numbers. Data are from 3 independent experiments (n=6 mice per genotype). (H) Measurements of oxygen consumption rate (OCR), indicative of mitochondrial oxidative phosphorylation in bone marrow LSK and MEPs. OCR values were normalized to cell numbers. Data are from 3 independent experiments, n=6 mice per genotype. (I) Glucose uptake capacity of LSK and MEPs in bone marrow and spleen as measured by mean fluorescence intensity (MFI) of 2-NBDG fluorescence (n=6 mice per genotype). (J) Number of mitochondria per cell in bone marrow LSK and MEP cells as determined by transmission electron microscopy (TEM) (n=3 samples per genotype and 60-100 cells per genotype). (K) Mitochondrial DNA copy number in bone marrow LT-HSCs, MPPs and MEPs as measured by qPCR (n=3 per genotype). (L) Mitochondrial DNA copy number in peripheral blood of MPN patients as measured by qPCR presented as violin density plots. The horizontal width of the plots shows the density of the data along the y-axis. All data are presented as mean ± SEM. One-way ANOVA analyses followed by Tukey's multiple comparison tests were used for multiple group comparisons. *P < .05; **P < .01; ***P < .001. See also Supplemental Figure S4 and S5.

Figure 5. Increased incorporation of glucose carbon through glycolysis and the pentose phosphate pathway in mutant *JAK2* expressing hematopoietic stem and progenitor cells. (A) Schematic of glucose labeling and tracing in bone marrow LSK and MEP cells. FACS sorted LSK and MEPs were cultured with [U-$^{13}C_6$] D-glucose for 8

hours and analyzed by ion chromatography–Fourier transform mass spectrometry (IC-FTMS) to determine the fate of labeled carbon atoms derived from glucose in various downstream metabolites. (B) Bar graphs depicting the levels (μmoles per gram protein) of glucose-derived ^{13}C containing isotopologues of metabolites in glycolysis and pentose phosphate pathways. LSK and MEP cells are collected and pooled from 9-12 mice of matching genotype as one replicate. Data are from two independent experiments. Insert showing the key rate-limiting step in glycolysis in which the activity of Pfkfb enzyme potentiates activity of rate limiting enzyme phosphofructokinase (Pfk) through generation of fructose 2,6 biphosphate from fructose 6 phosphate. 3PO is a specific pharmacological inhibitor of Pfkfb3 isoform. (C) *Pfkfb1-4* mRNA expression in MEP cells (n=3 per genotype). (D**)** Pfkfb3 protein expression in bone marrow LSK and MEP cells as measured by intracellular FACS (n=3 per genotype). (E) Graphical representation of increased glycolysis rate limiting step involving conversion of F6P to F 1,6 BP and its positive regulator PFKFB3, which can be inhibited by 3PO. All data are presented as mean ± SEM. *P < .05; **P < .01. See also Supplemental Figure S6. G6P, glucose 6-phosphate; F6P, fructose 6-phosphate; FBP, fructose 1,6-bisphosphate; DHAP, dihydroxyacetone phosphate; G3P, glyceraldehyde 3-phosphate; 6PGL, 6-Phosphogluconolactone; 6PG, 6-phosphogluconate; Ru5P, ribulose 5-phosphate; R5P, ribose 5-phosphate; Xu5P, xylulose 5-phosphate; PRPP, phosphoribosyl pyrophosphate; S7P, sedoheptulose 7-phosphate; E4P, erythrose 4-phosphate.

Figure 6. Dual treatment with 3PO and Ruxolitinib induces cell proliferation arrest and apoptosis in human cell lines expressing *JAK2*-V617F by altering redox homeostasis. (A) Apoptosis rate was determined by percent of Annexin V^+ cells in indicated human myeloid leukemia cells after treatment with 3PO and/or Ruxolitinib for 48 hours (n=3 independent experiments). (B) Cell proliferation was determined by percent of $Ki67^+$ cells in indicated human myeloid leukemia cells in the presence of 3PO and/or Ruxolitinib for 48 hours (n=3 independent experiments). (C) Measurements of extracellular acidification rate (ECAR), indicative of glycolytic rates, in SET2, HEL UKE1, K562 cells after treatment with 3PO and/or Ruxolitinib for 12-16 hours (n=3 independent experiments). (D) Measurements of oxygen consumption rate (OCR), indicative of mitochondrial oxidative phosphorylation, in indicated cells after treatment with 3PO and/or Ruxolitinib for 12-16 hours (n=3 independent experiments). (E) Total ROS levels in SET2 cells after treatment with 3PO and/or Ruxolitinib for 24 hours. Cells were pretreated with

1.5 mM N-Acetyl-Cysteine (NAC) for 6 hours. Data was normalized to vehicle treated control (n=3 independent experiments). (F and G) Apoptosis rate (F) and cell proliferation (G) was determined in SET2 cells treated with 3PO and/or Ruxolitinib and/or NAC for 48 hours. Cells were pre-treated with NAC for 6 hours. Normalized values to vehicle treated controls are shown. (H and I) Ratio of GSH/GSSG (H) and NADPH levels (I) in SET2 cells treated with 3PO and/or Ruxolitinib for 12 hours. Cells were pre-treated with NAC for 6 hours. Normalized values to vehicle treated controls are shown. All data are presented as mean ± SEM. Two-way ANOVA with subsequent Bonferroni post-test was used. *P < .05; **P < .01; ***P < .001. See also Figure S7.

Figure 7. Combined targeting of elevated glycolysis and mutant JAK2 activity elicited additive effects *in vivo*. (A) Schematic of long-term 3PO and Ruxolitinib treatment. Competitive bone marrow transplant recipient mice were induced with tamoxifen (TAM) to activate the *JAK2-VF* and *JAK2-E12* mutations. 4 (for *E12*) or 8 (for *VF*) weeks later the treatment regimen was initiated. Mice were treated with vehicle, 3PO (50mg/kg, i.p) alone or in combination with Ruxolitinib (60mg/kg, oral) every day for 8 weeks. (B) Representative pictures and weights of spleen from mice treated with vehicle or 3PO and/or Ruxolitinib (n=6 mice per genotype). (C) Weight of eWAT in 3PO and/or Ruxolitinib treated mice (n=6 mice per genotype). (D) Time course of non-fasting blood glucose levels in 3PO and/or Ruxolitinib treated mice (n=6 mice per genotype). (E) Glucose tolerance test in 3PO and/or Ruxolitinib treated *VF* (left) and *E12* (right) mice (n=6 mice per genotype). (F) Peripheral blood cell counts (upper panel) and frequencies of GFP positive hematopoietic cells in peripheral blood (lower panel) in 3PO and/or Ruxolitinib treated mice at indicated time points (n=6 mice per genotype). (G) Blood glucose levels in PV patients with or without cytoreductive therapy. Cytoreductive drugs were hydroxyurea (n=19), pegylated interferon-α (n=1), ruxolitinib (n=3), and anagrelide (n=1). (H) Schematic drawing depicting the metabolic changes in hematopoietic and non-hematopoietic tissues induced by expression of mutant *JAK2* in hematopoietic cells. Metabolic changes and MPN are primarily driven by the expression of mutant *JAK2* in hematopoietic cells. High glucose diet (HGD) promotes proliferation of the JAK2 mutant clone and accelerates MPN phenotype, whereas Ruxolitinib, 3PO and high fat diet (HFD) reduce the MPN manifestations. Note that some changes in metabolism are directly affecting the JAK2 mutant hematopoietic cells, whereas other changes (e.g. lipolysis) are indirect consequences of the general energy crisis and/or the inflammatory mediators

secreted by the JAK2 mutant cells. One-way ANOVA analyses followed by Tukey's multiple comparison tests were used for multiple group comparisons or Two-way ANOVA with subsequent Bonferroni post-test or two-tailed unpaired t-test (G) was used. All data are presented as mean ± SEM. *P < .05; **P < .01. See also Figure S8.

Figure 1

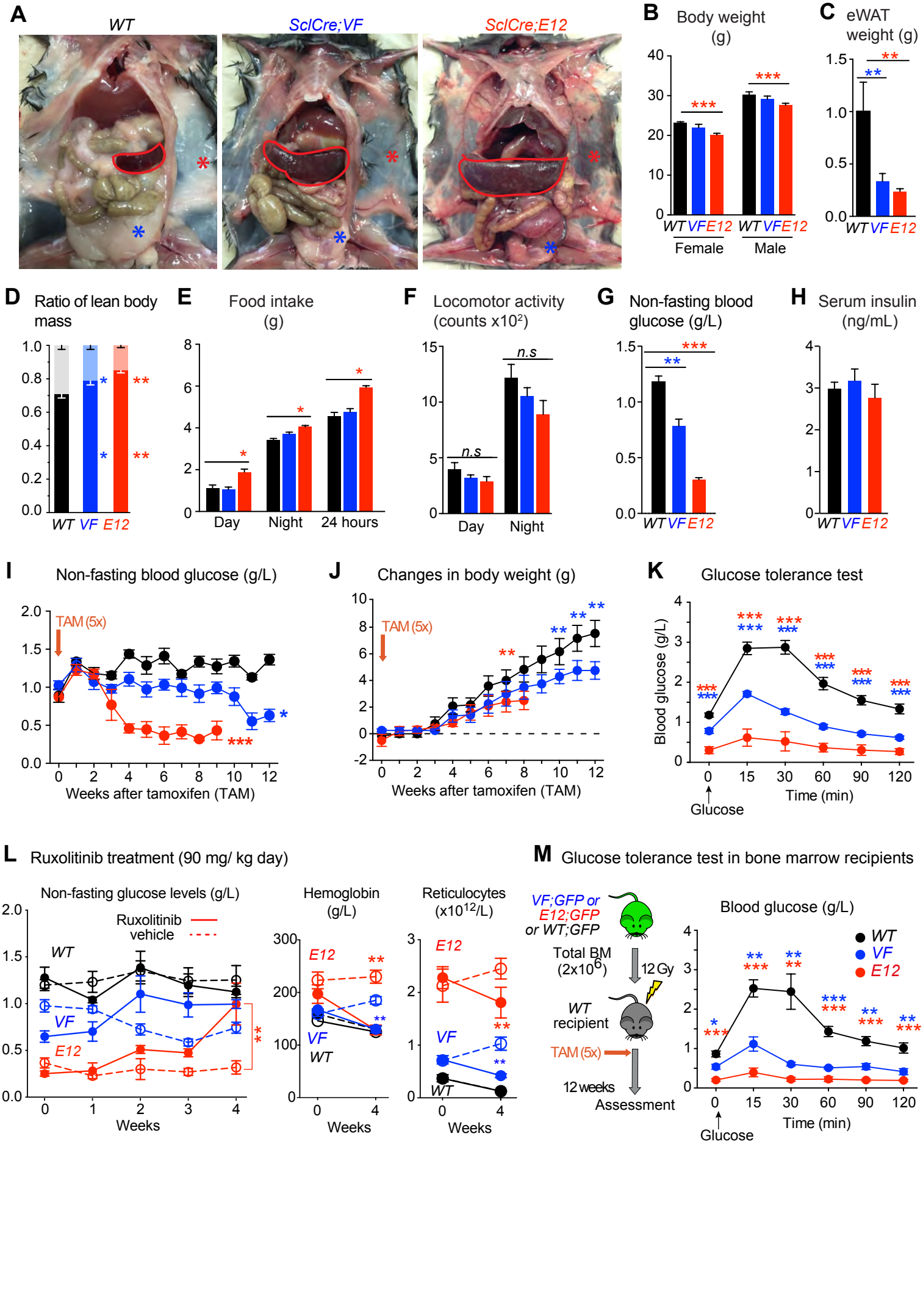
A
WT
SclCre;VF
SclCre;E12
B
Body weight (g)
WT VF E12 WT VF E12
Female
Male
C
eWAT weight (g)
WT VF E12
D
Ratio of lean body mass
WT VF E12
E
Food intake (g)
Day
Night
24 hours
F
Locomotor activity (counts x10²)
n.s
Day
Night
G
Non-fasting blood glucose (g/L)
WT VF E12
H
Serum insulin (ng/mL)
WT VF E12
I
Non-fasting blood glucose (g/L)
TAM (5x)
Weeks after tamoxifen (TAM)
J
Changes in body weight (g)
TAM (5x)
Weeks after tamoxifen (TAM)
K
Glucose tolerance test
Blood glucose (g/L)
Glucose
Time (min)
L
Ruxolitinib treatment (90 mg/ kg day)
Non-fasting glucose levels (g/L)
Ruxolitinib
vehicle
WT
VF
E12
Weeks
Hemoglobin (g/L)
Reticulocytes (x10¹²/L)
M
Glucose tolerance test in bone marrow recipients
VF;GFP or E12;GFP or WT;GFP
Total BM (2x10⁶)
12 Gy
WT recipient
TAM (5x)
12 weeks
Assessment
Blood glucose (g/L)
WT
VF
E12
Glucose
Time (min)

Figure 2

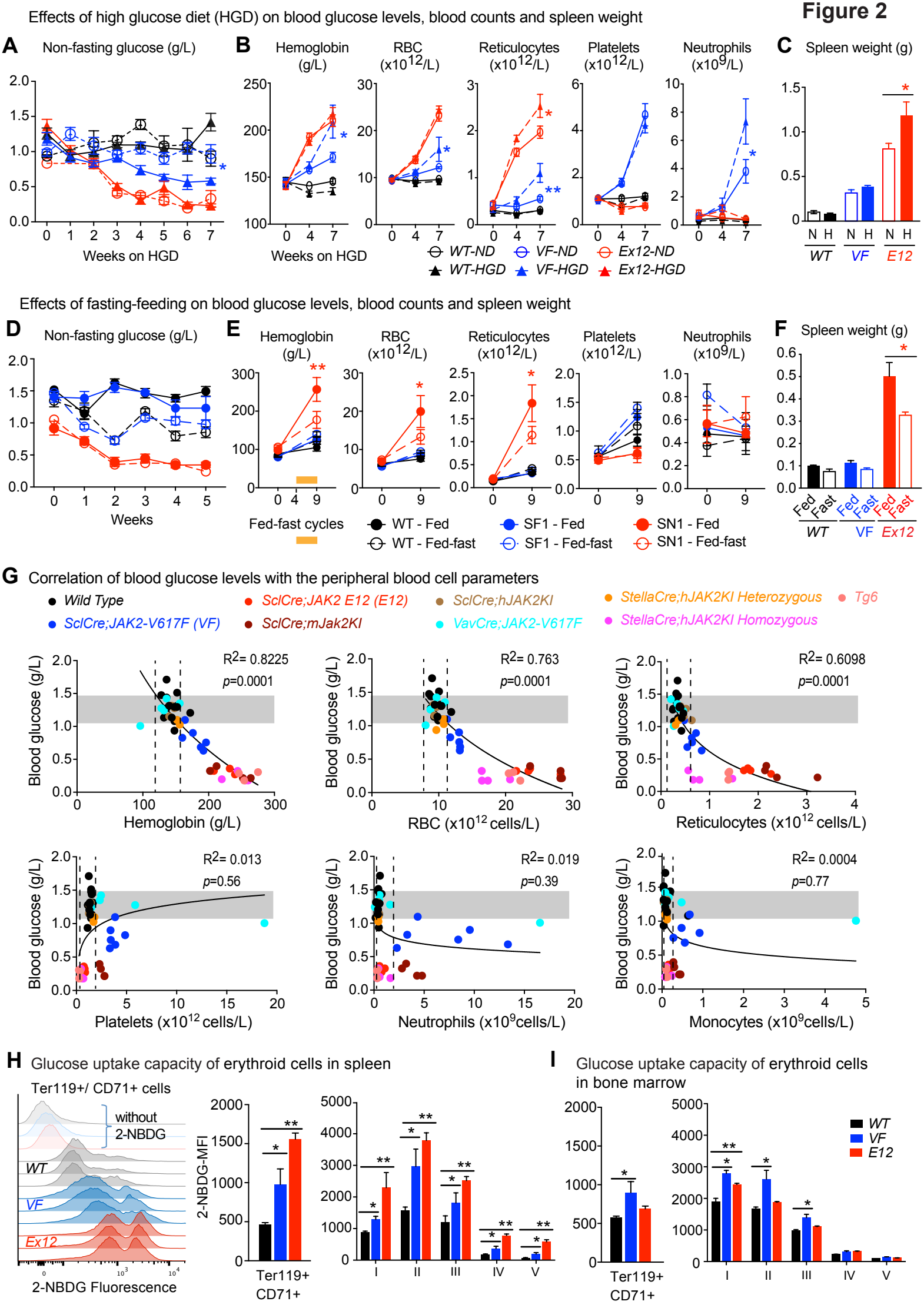
Effects of high glucose diet (HGD) on blood glucose levels, blood counts and spleen weight
A
Non-fasting glucose (g/L)
Weeks on HGD
B
Hemoglobin (g/L)
RBC (x10^12/L)
Reticulocytes (x10^12/L)
Platelets (x10^12/L)
Neutrophils (x10^9/L)
Weeks on HGD
WT-ND
WT-HGD
VF-ND
VF-HGD
Ex12-ND
Ex12-HGD
C
Spleen weight (g)
N H N H N H
WT VF E12
Effects of fasting-feeding on blood glucose levels, blood counts and spleen weight
D
Non-fasting glucose (g/L)
Weeks
E
Hemoglobin (g/L)
RBC (x10^12/L)
Reticulocytes (x10^12/L)
Platelets (x10^12/L)
Neutrophils (x10^9/L)
Fed-fast cycles
WT - Fed
WT - Fed-fast
SF1 - Fed
SF1 - Fed-fast
SN1 - Fed
SN1 - Fed-fast
F
Spleen weight (g)
Fed Fast Fed Fast Fed Fast
WT VF Ex12
G
Correlation of blood glucose levels with the peripheral blood cell parameters
Wild Type
SclCre;JAK2 E12 (E12)
SclCre;hJAK2KI
StellaCre;hJAK2KI Heterozygous
Tg6
SclCre;JAK2-V617F (VF)
SclCre;mJak2KI
VavCre;JAK2-V617F
StellaCre;hJAK2KI Homozygous
Blood glucose (g/L)
R2= 0.8225
p=0.0001
Hemoglobin (g/L)
R2= 0.763
p=0.0001
RBC (x10^12 cells/L)
R2= 0.6098
p=0.0001
Reticulocytes (x10^12 cells/L)
R2= 0.013
p=0.56
Platelets (x10^12 cells/L)
R2= 0.019
p=0.39
Neutrophils (x10^9cells/L)
R2= 0.0004
p=0.77
Monocytes (x10^9cells/L)
H
Glucose uptake capacity of erythroid cells in spleen
Ter119+/ CD71+ cells
without 2-NBDG
WT
VF
Ex12
2-NBDG Fluorescence
2-NBDG-MFI
Ter119+ CD71+
I
Glucose uptake capacity of erythroid cells in bone marrow
WT
VF
E12
Ter119+ CD71+

Figure 3

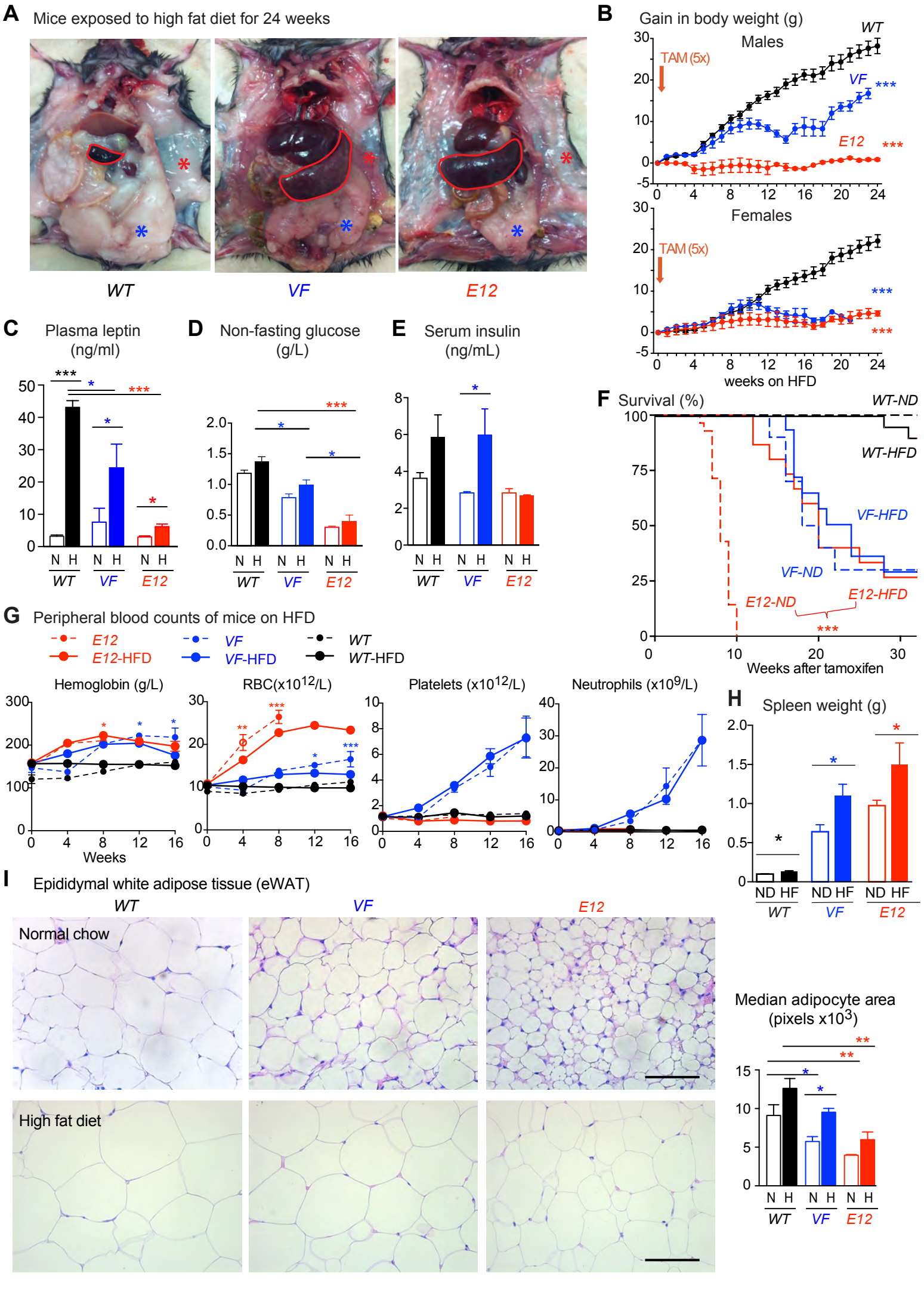
A
Mice exposed to high fat diet for 24 weeks
WT
VF
E12
B
Gain in body weight (g)
Males
TAM (5x)
WT
VF
E12
***
Females
weeks on HFD
C
Plasma leptin (ng/ml)
D
Non-fasting glucose (g/L)
E
Serum insulin (ng/mL)
N H
F
Survival (%)
WT-ND
WT-HFD
VF-HFD
VF-ND
E12-ND
E12-HFD
Weeks after tamoxifen
G
Peripheral blood counts of mice on HFD
E12
E12-HFD
VF
VF-HFD
WT
WT-HFD
Hemoglobin (g/L)
RBC(x10^12/L)
Platelets (x10^12/L)
Neutrophils (x10^9/L)
Weeks
H
Spleen weight (g)
ND HF
I
Epididymal white adipose tissue (eWAT)
Normal chow
High fat diet
Median adipocyte area (pixels x10^3)

Figure 4

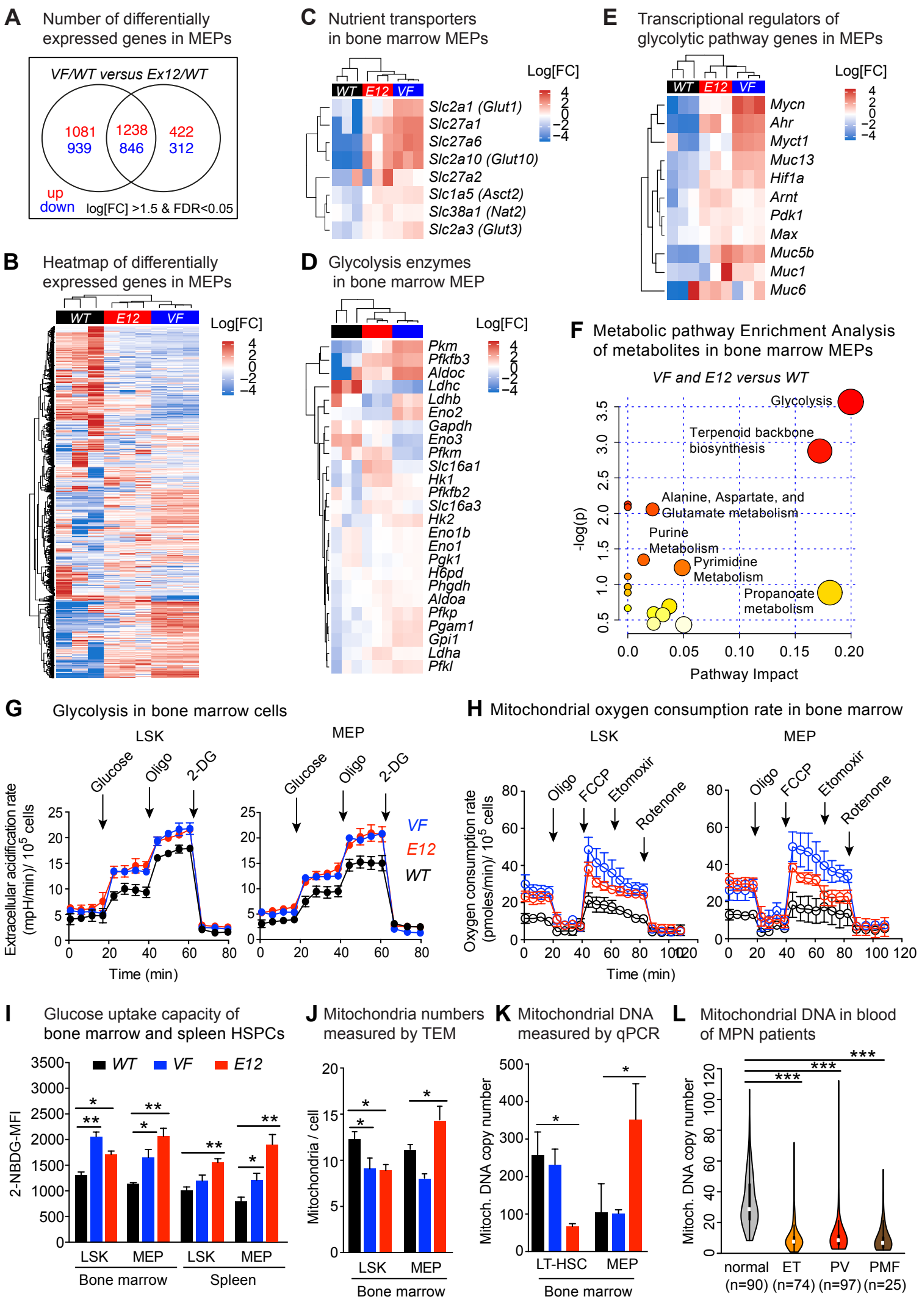
A
Number of differentially expressed genes in MEPs
VF/WT versus Ex12/WT
1081
939
1238
846
422
312
up
down
log[FC] >1.5 & FDR<0.05
B
Heatmap of differentially expressed genes in MEPs
WT
E12
VF
Log[FC]
4
2
0
−2
−4
C
Nutrient transporters in bone marrow MEPs
Slc2a1 (Glut1)
Slc27a1
Slc27a6
Slc2a10 (Glut10)
Slc27a2
Slc1a5 (Asct2)
Slc38a1 (Nat2)
Slc2a3 (Glut3)
D
Glycolysis enzymes in bone marrow MEP
Pkm
Pfkfb3
Aldoc
Ldhc
Ldhb
Eno2
Gapdh
Eno3
Pfkm
Slc16a1
Hk1
Pfkfb2
Slc16a3
Hk2
Eno1b
Eno1
Pgk1
H6pd
Phgdh
Aldoa
Pfkp
Pgam1
Gpi1
Ldha
Pfkl
E
Transcriptional regulators of glycolytic pathway genes in MEPs
Mycn
Ahr
Myct1
Muc13
Hif1a
Arnt
Pdk1
Max
Muc5b
Muc1
Muc6
F
Metabolic pathway Enrichment Analysis of metabolites in bone marrow MEPs
VF and E12 versus WT
Glycolysis
Terpenoid backbone biosynthesis
Alanine, Aspartate, and Glutamate metabolism
Purine Metabolism
Pyrimidine Metabolism
Propanoate metabolism
-log(p)
Pathway Impact
G
Glycolysis in bone marrow cells
LSK
MEP
Glucose
Oligo
2-DG
VF
E12
WT
Extracellular acidification rate (mpH/min)/ 10^5 cells
Time (min)
H
Mitochondrial oxygen consumption rate in bone marrow
LSK
MEP
Oligo
FCCP
Etomoxir
Rotenone
Oxygen consumption rate (pmoles/min)/ 10^5 cells
Time (min)
I
Glucose uptake capacity of bone marrow and spleen HSPCs
WT
VF
E12
2-NBDG-MFI
LSK
MEP
LSK
MEP
Bone marrow
Spleen
J
Mitochondria numbers measured by TEM
Mitochondria / cell
LSK
MEP
Bone marrow
K
Mitochondrial DNA measured by qPCR
Mitoch. DNA copy number
LT-HSC
MEP
Bone marrow
L
Mitochondrial DNA in blood of MPN patients
Mitoch. DNA copy number
normal (n=90)
ET (n=74)
PV (n=97)
PMF (n=25)

Figure 5

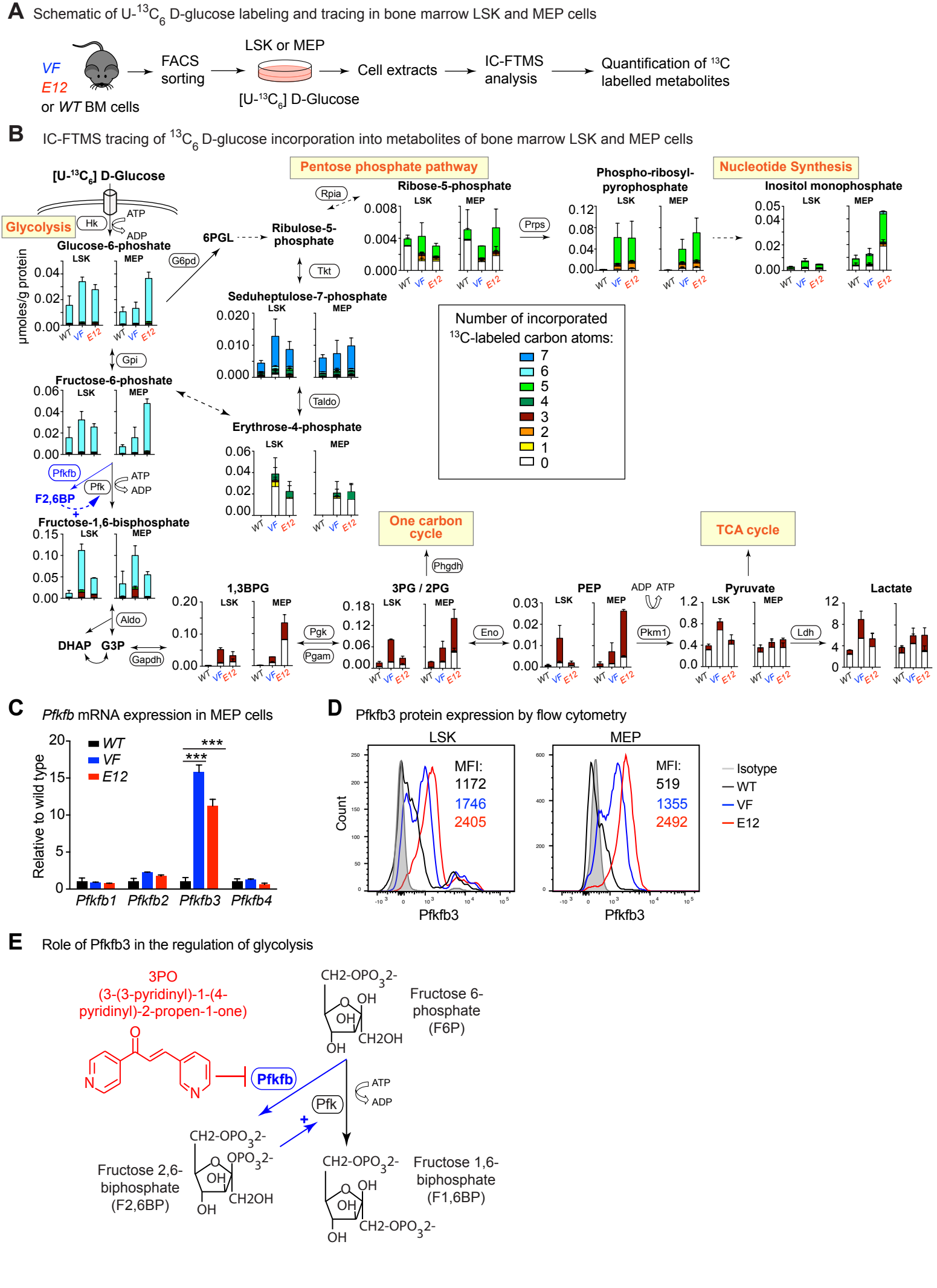
A
Schematic of U-13C6 D-glucose labeling and tracing in bone marrow LSK and MEP cells
VF
E12
or WT BM cells
FACS sorting
LSK or MEP
[U-13C6] D-Glucose
Cell extracts
IC-FTMS analysis
Quantification of 13C labelled metabolites
B
IC-FTMS tracing of 13C6 D-glucose incorporation into metabolites of bone marrow LSK and MEP cells
[U-13C6] D-Glucose
Glycolysis
Hk
ATP
ADP
Glucose-6-phoshate
G6pd
6PGL
Pentose phosphate pathway
Rpia
Ribose-5-phosphate
Ribulose-5-phosphate
Tkt
Seduheptulose-7-phosphate
Taldo
Erythrose-4-phosphate
Prps
Phospho-ribosyl-pyrophosphate
Nucleotide Synthesis
Inositol monophosphate
Gpi
Fructose-6-phoshate
Pfkfb
Pfk
F2,6BP
Fructose-1,6-bisphosphate
Aldo
DHAP
G3P
Gapdh
1,3BPG
Pgk
Pgam
3PG / 2PG
Phgdh
One carbon cycle
Eno
PEP
ADP ATP
Pkm1
Pyruvate
TCA cycle
Ldh
Lactate
LSK
MEP
WT
VF
E12
µmoles/g protein
Number of incorporated 13C-labeled carbon atoms:
7
6
5
4
3
2
1
0
C
Pfkfb mRNA expression in MEP cells
WT
VF
E12
Relative to wild type
***
Pfkfb1
Pfkfb2
Pfkfb3
Pfkfb4
D
Pfkfb3 protein expression by flow cytometry
LSK
MEP
Count
MFI:
1172
1746
2405
519
1355
2492
Isotype
WT
VF
E12
Pfkfb3
E
Role of Pfkfb3 in the regulation of glycolysis
3PO
(3-(3-pyridinyl)-1-(4-pyridinyl)-2-propen-1-one)
Pfkfb
Pfk
ATP
ADP
Fructose 6-phosphate (F6P)
Fructose 2,6-biphosphate (F2,6BP)
Fructose 1,6-biphosphate (F1,6BP)
CH2-OPO3 2-
OH
CH2OH

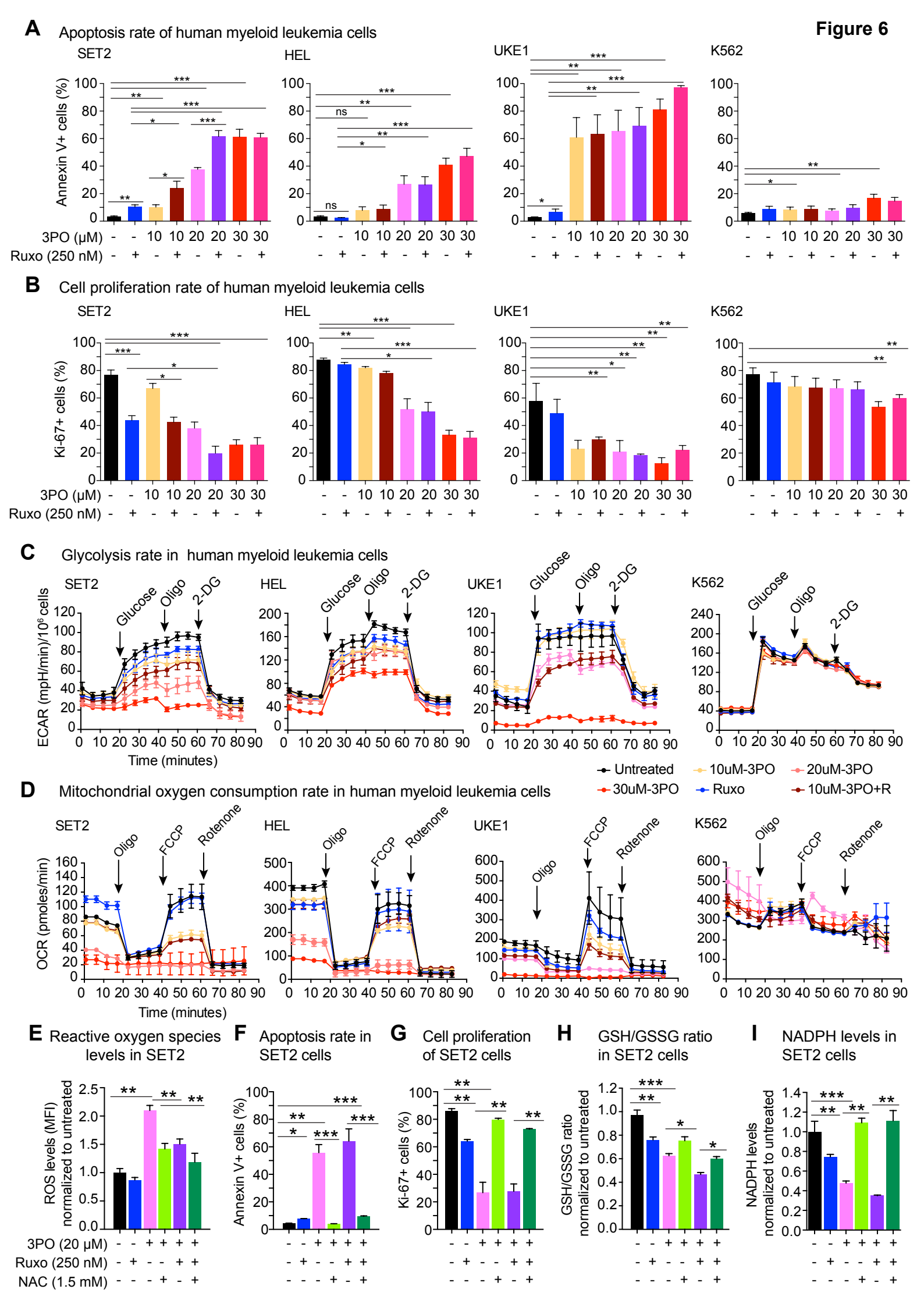
A
Apoptosis rate of human myeloid leukemia cells
SET2
HEL
UKE1
K562
Annexin V+ cells (%)
3PO (μM)
Ruxo (250 nM)
B
Cell proliferation rate of human myeloid leukemia cells
Ki-67+ cells (%)
C
Glycolysis rate in human myeloid leukemia cells
ECAR (mpH/min)/10^6 cells
Glucose
Oligo
2-DG
Time (minutes)
Untreated
10uM-3PO
20uM-3PO
30uM-3PO
Ruxo
10uM-3PO+R
D
Mitochondrial oxygen consumption rate in human myeloid leukemia cells
OCR (pmoles/min)
FCCP
Rotenone
E
Reactive oxygen species levels in SET2
ROS levels (MFI) normalized to untreated
NAC (1.5 mM)
F
Apoptosis rate in SET2 cells
G
Cell proliferation of SET2 cells
H
GSH/GSSG ratio in SET2 cells
GSH/GSSG ratio normalized to untreated
I
NADPH levels in SET2 cells
NADPH levels normalized to untreated

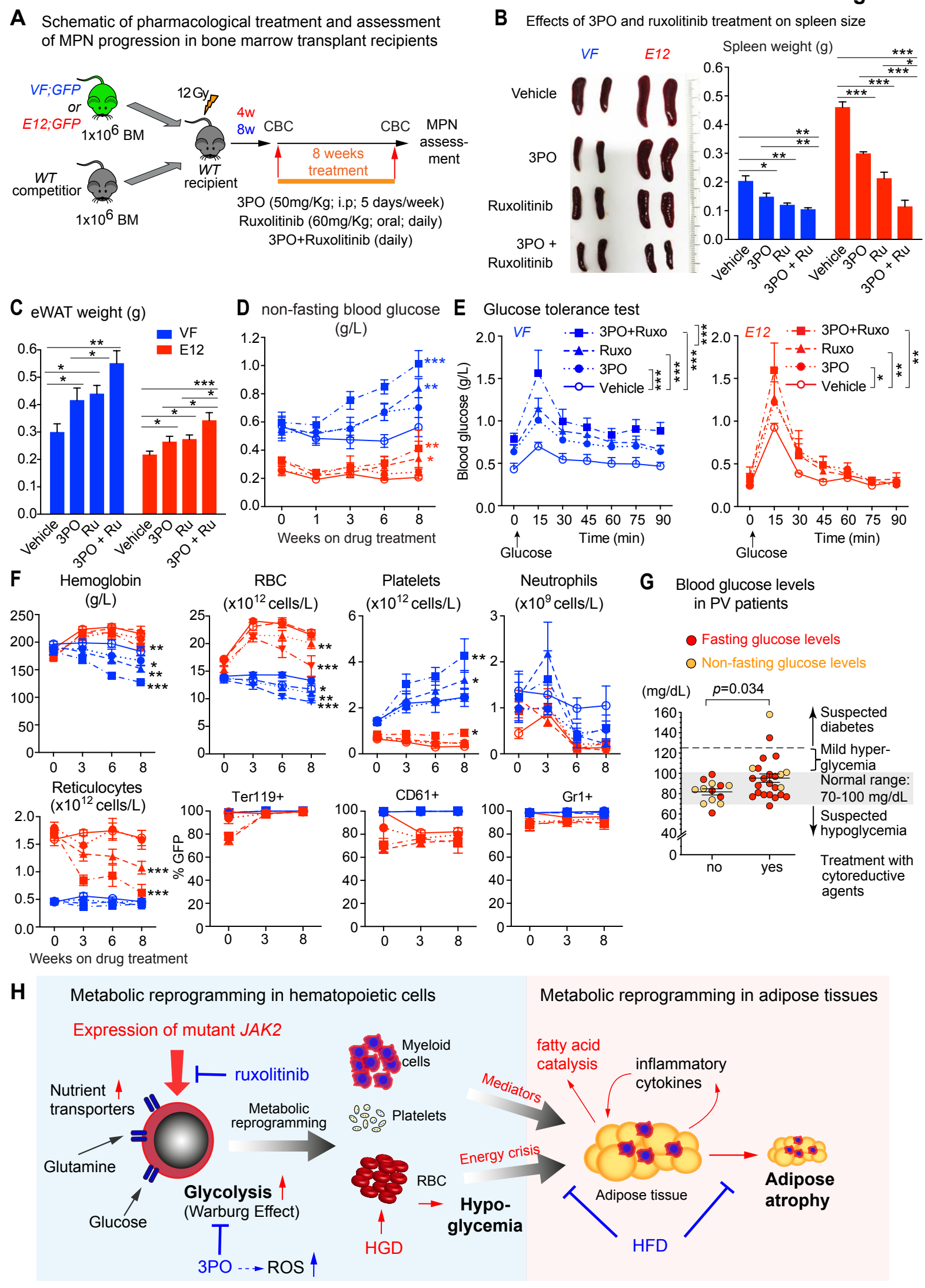
A
Schematic of pharmacological treatment and assessment of MPN progression in bone marrow transplant recipients
VF;GFP or E12;GFP
1x10^6 BM
12 Gy
WT recipient
WT competitor
1x10^6 BM
4w
8w
CBC
CBC
8 weeks treatment
MPN assess-ment
3PO (50mg/Kg; i.p; 5 days/week)
Ruxolitinib (60mg/Kg; oral; daily)
3PO+Ruxolitinib (daily)
B
Effects of 3PO and ruxolitinib treatment on spleen size
VF
E12
Vehicle
3PO
Ruxolitinib
3PO + Ruxolitinib
Spleen weight (g)
Vehicle
3PO
Ru
3PO + Ru
C
eWAT weight (g)
VF
E12
D
non-fasting blood glucose (g/L)
Weeks on drug treatment
E
Glucose tolerance test
VF
E12
3PO+Ruxo
Ruxo
3PO
Vehicle
Blood glucose (g/L)
Time (min)
Glucose
F
Hemoglobin (g/L)
RBC (x10^12 cells/L)
Platelets (x10^12 cells/L)
Neutrophils (x10^9 cells/L)
Reticulocytes (x10^12 cells/L)
Ter119+
CD61+
Gr1+
% GFP
Weeks on drug treatment
G
Blood glucose levels in PV patients
Fasting glucose levels
Non-fasting glucose levels
(mg/dL)
p=0.034
no
yes
Suspected diabetes
Mild hyper-glycemia
Normal range: 70-100 mg/dL
Suspected hypoglycemia
Treatment with cytoreductive agents
H
Metabolic reprogramming in hematopoietic cells
Expression of mutant JAK2
ruxolitinib
Nutrient transporters
Glutamine
Glucose
Metabolic reprogramming
Glycolysis (Warburg Effect)
3PO
ROS
Myeloid cells
Platelets
RBC
HGD
Hypo-glycemia
Mediators
Energy crisis
Metabolic reprogramming in adipose tissues
fatty acid catalysis
inflammatory cytokines
Adipose tissue
HFD
Adipose atrophy

Supplemental Figure S1

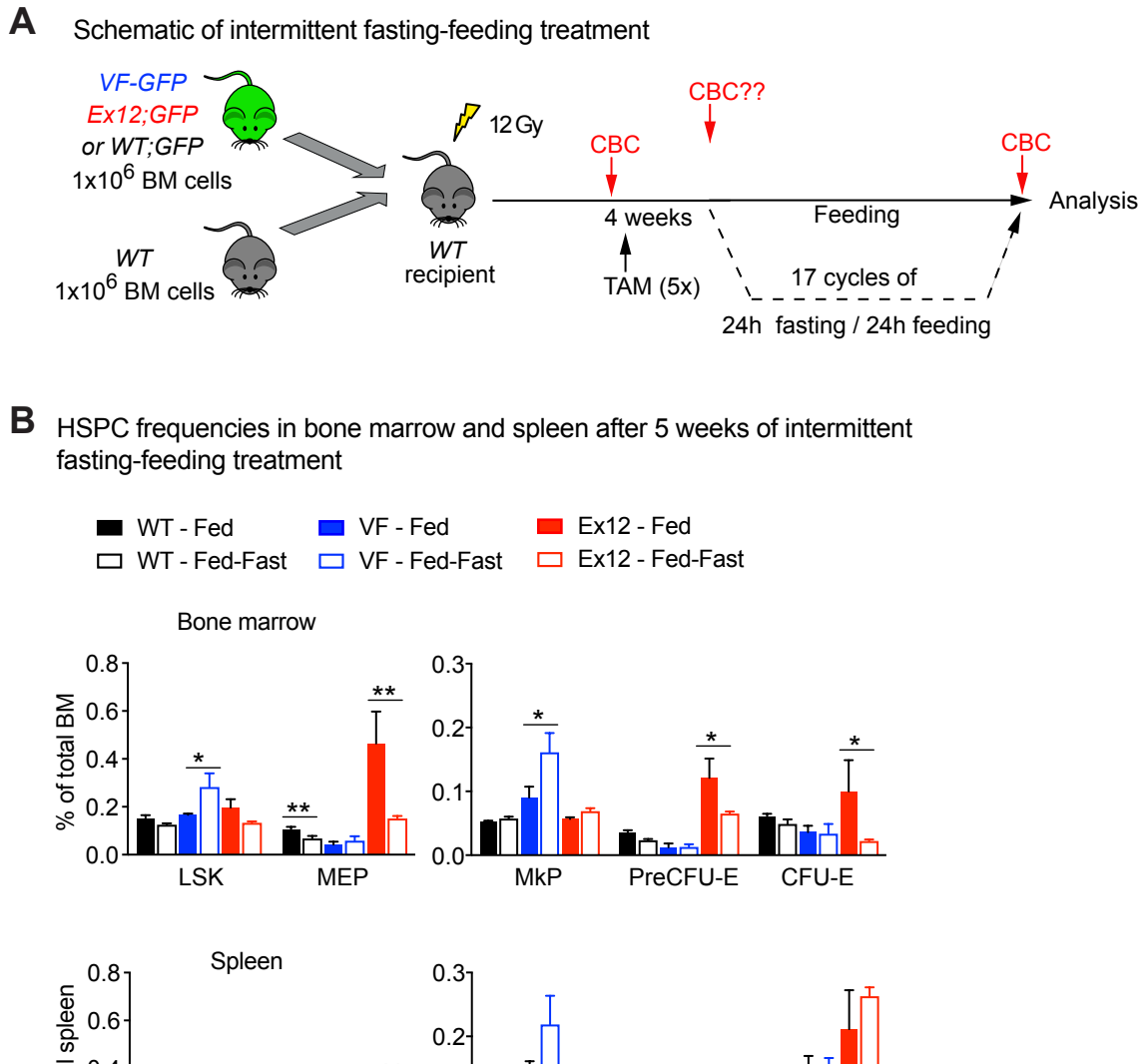

Supplemental Figure S1. Reducing energy supply through fasting has beneficial effects in reducing MPN progression in MPN mice. (A) MPN induction and prolonged fasting scheme. Bone marrow transplant recipient mice were treated with tamoxifen (TAM) to activate the JAK2-VF and JAK2-E12 mutations. Four weeks after TAM injections, mice were fed normally or subjected to fasting with 17 cycles of 1d-fasting/1d-feeding regimen. (B) Bar graphs showing the frequency of donor derived HSPCs and megakaryocyte and erythroid committed progenitors in BM (upper panel) and spleen (lower panel) of indicated mice (n=4-5 mice per genotype). All data are presented as mean ± SEM. One-way ANOVA analyses followed by Tukey's multiple comparison tests were used. *P < .05; **P < .01.

Supplemental Figure S2

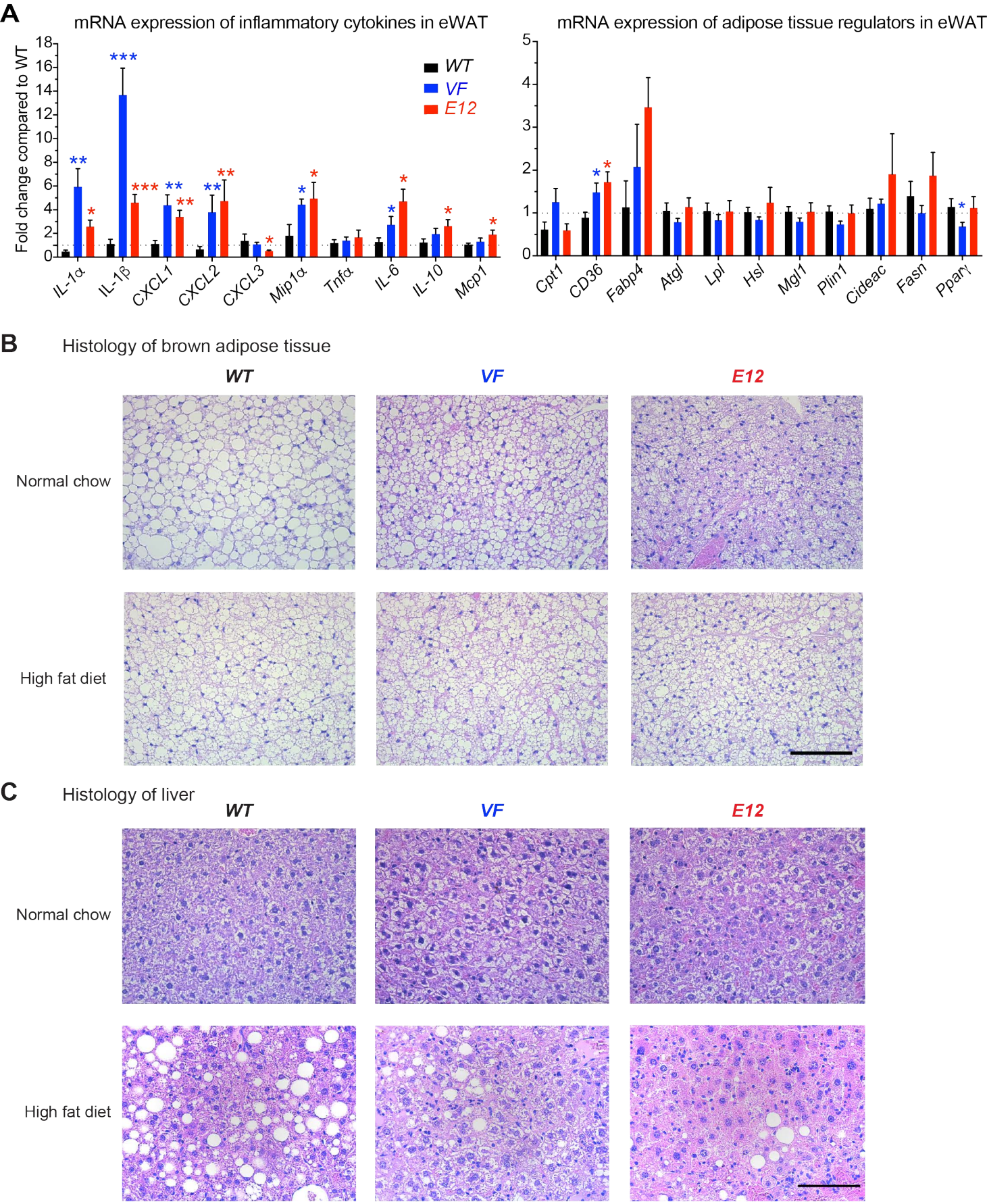

Supplemental Figure S2: A) Quantitative RT-PCR analyses of inflammatory cytokines (left) and adipose tissue regulators mRNA expression in eWAT (n= 5-6 mice per genotype). (B and C) Representative images of hematoxylin and eosin (H&E) staining of brown adipose tissue (B) and liver (C) from normal chow or high fat diet treated mice (n= 4-5 mice per genotype and treatment). Scale bars=100μm. All data are presented as mean ± SEM. One-way ANOVA analyses followed by Tukey's multiple comparison tests were used for multiple group comparisons.*P < .05; **P < .01; ***P < .001.

Supplementary Figure S3

A Differentially regulated pathways in MEP cells by Ingenuity Pathway Analysis (IPA)

VF mice compared to wildtype controls

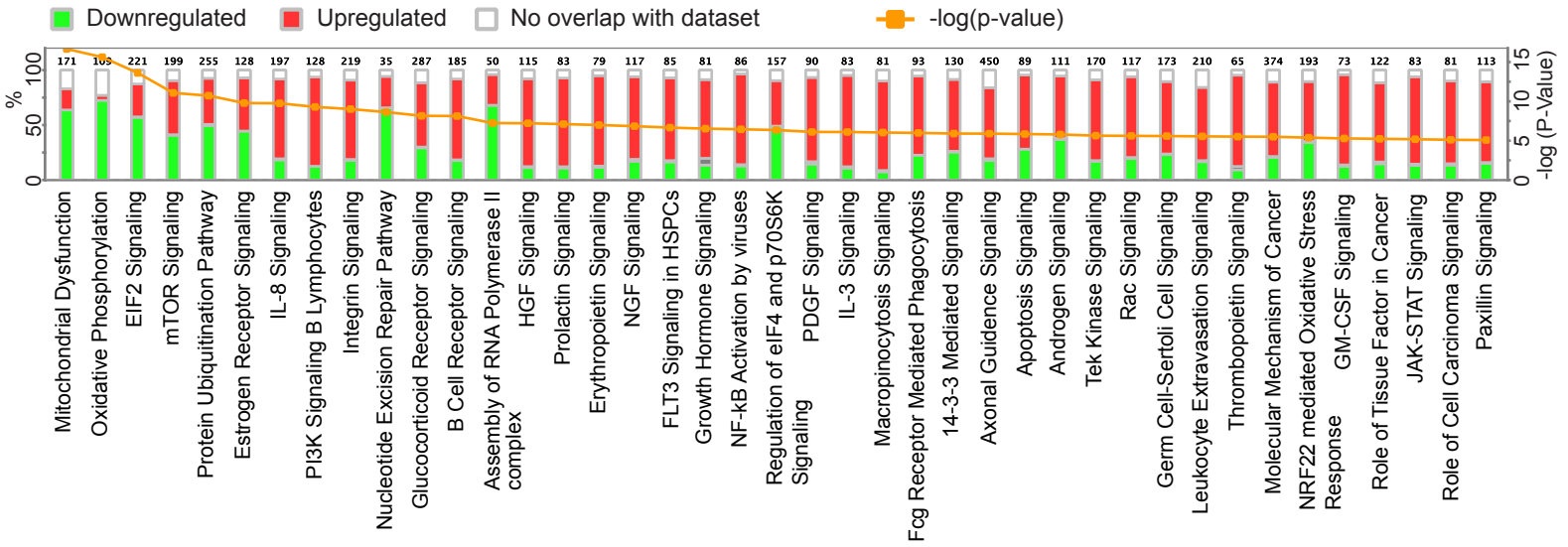

E12 mice compared to wildtype controls

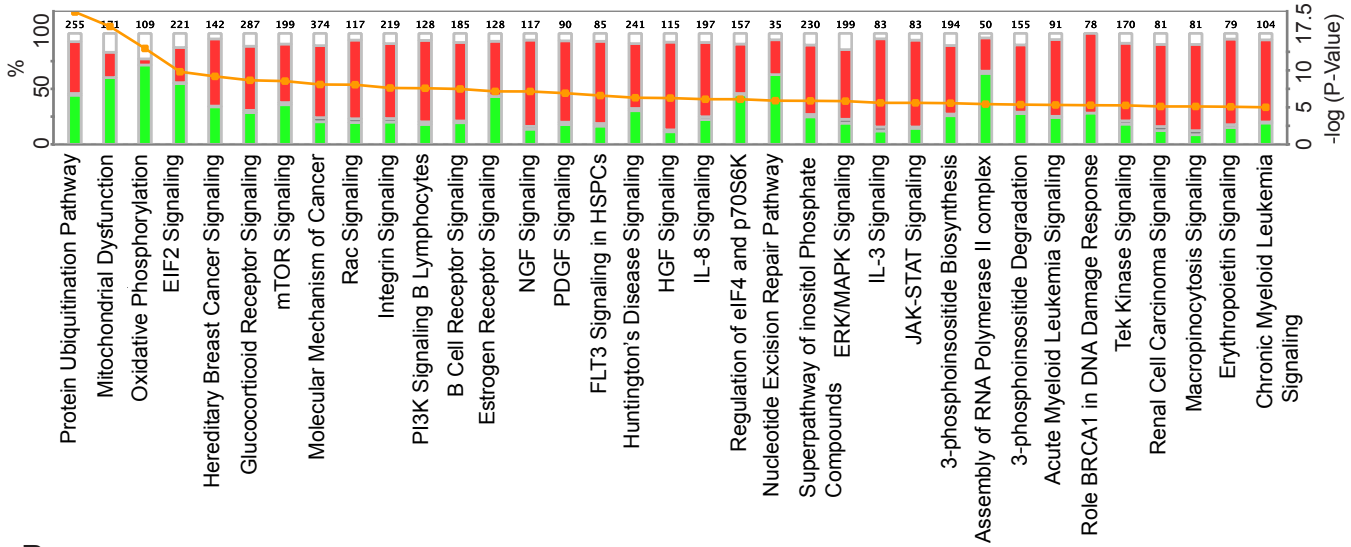

B Gene Set Enrichement Analysis (GSEA)

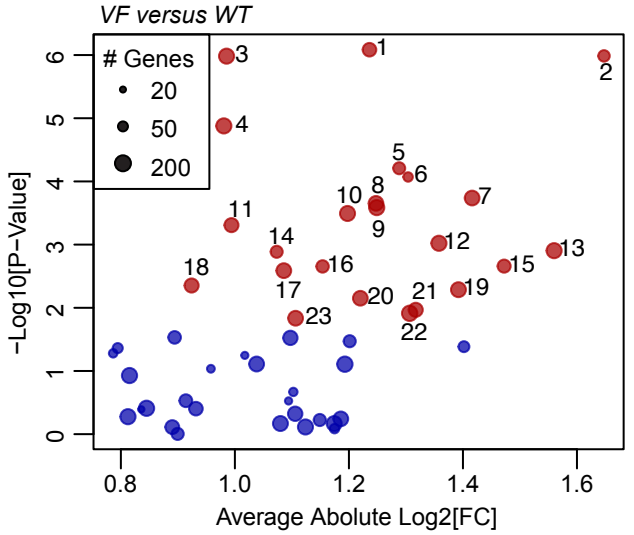

1 UV response down
2 IL6 JAK STAT3 Signaling
3 Oxidative Phosphorylation
4 Mitotic Spindle
5 Androgen Response
6 TGF Beta Signaling
7 Inflammatory Response
8 Apical Junction
9 Allograft rejection
10 TNFa Signaling via NFkB
11 DNA Repair
12 IL2 STAT5 Signaling
13 Heme Metabolism
14 Protein Secretion
15 Coagulation
16 PI3K AKT mTOR Signaling
17 Estrogen Response early
18 Fatty Acid Metabolism
19 Hypoxia
20 Complement
21 Apoptosis
22 Interferon γ Response
23 Kras Signaling up

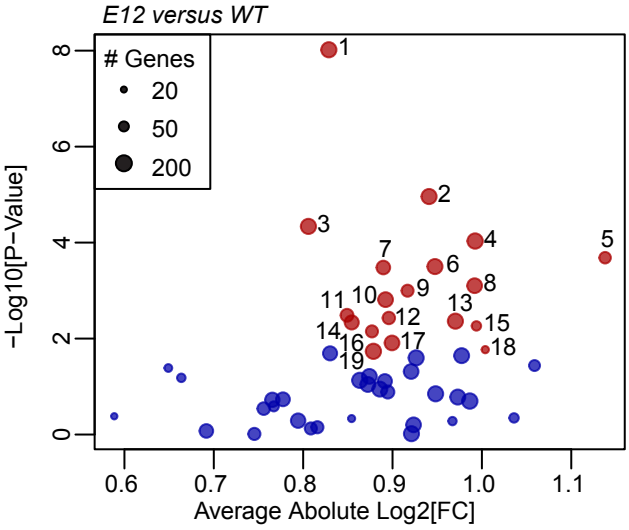

1 Mitotic Spindle
2 Oxidative Phosphorylation
3 G2M Checkpoint
4 mTORC1 Signaling
5 IL6 JAK STAT3 Signaling
6 TNFa Signaling Via NFkB
7 UV Response down
8 Inflammatory Response
9 Androgen Response
10 Estrogen Response early
11 Unfolded Protein Response
12 PI3K AKT mTOR Signaling
13 IL2 STAT5 Signaling
14 DNA Repair
15 TGF Beta Signaling
16 Protein Secretion
17 Apical Junction
18 Notch Signaling
19 E2F Targets

Supplemental Figure S4

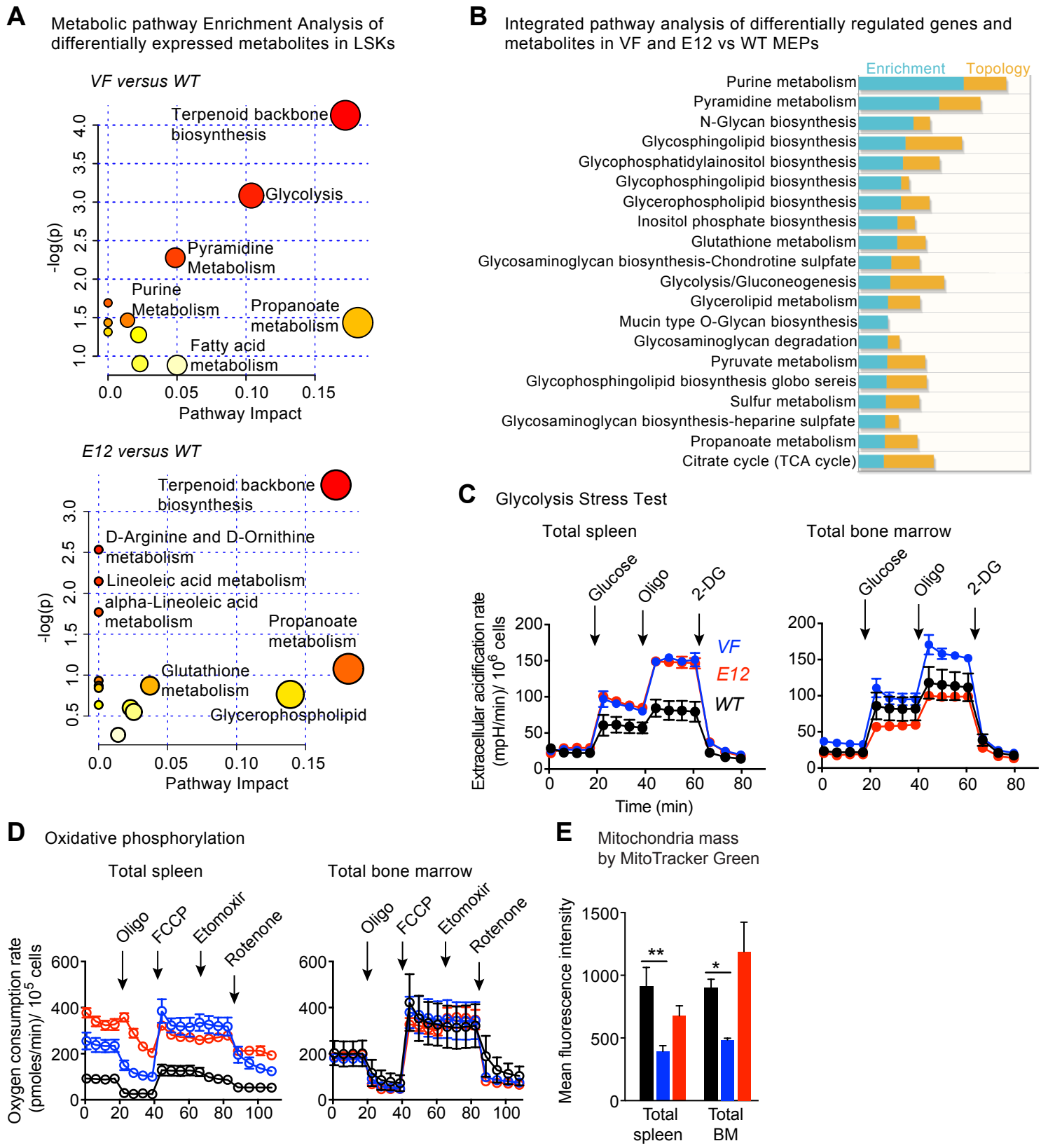

Supplemental Figure S4: Transcriptomic and metabolomic profiles of mutant JAK2 expressing hematopoietic stem and progenitor cells unveiled altered metabolic regulators. (A) Metabolic pathway enrichment analysis of significantly up-regulated metabolites in bone marrow MEPs from VF (upper panel) and E12 (lower panel) compared to WT mice as determined by MetaboloAnalyst 3.0 (n=3 per genotype). (B) Integrated pathway analysis of differentially regulated genes and metabolites in MEP cells from VF and E12 compared to WT mice. (C) Measurements of glycolytic rates from total spleen (left graph) and bone marrow cells (right graph). Extracellular acidification rate (ECAR) values were normalized to cell numbers. Data are from 3 independent experiments (n=6 mice per genotype). (D) Measurements of oxygen consumption rate (OCR), indicative of mitochondrial oxidative phosphorylation from total spleen (left graph) and bone marrow cells (right graph). OCR values were normalized to cell numbers. Data are from 3 independent experiments, n=6 mice per genotype. (E) Mitochondrial abundance as determined by the mean fluorescence intensity of MitoTrackerGreen in total spleen and bone marrow cells (n=5 mice per genotype). All data are presented as mean ± SEM. One-way ANOVA analyses followed by Tukey's multiple comparison tests were used for multiple group comparisons. *P < .05; **P < .01; ***P < .001.

Supplemental Figure S5

A IC-TFMS based tracing of ^{13}C from labelled U-$^{13}C_6$ D-glucose in LSK and MEP cells

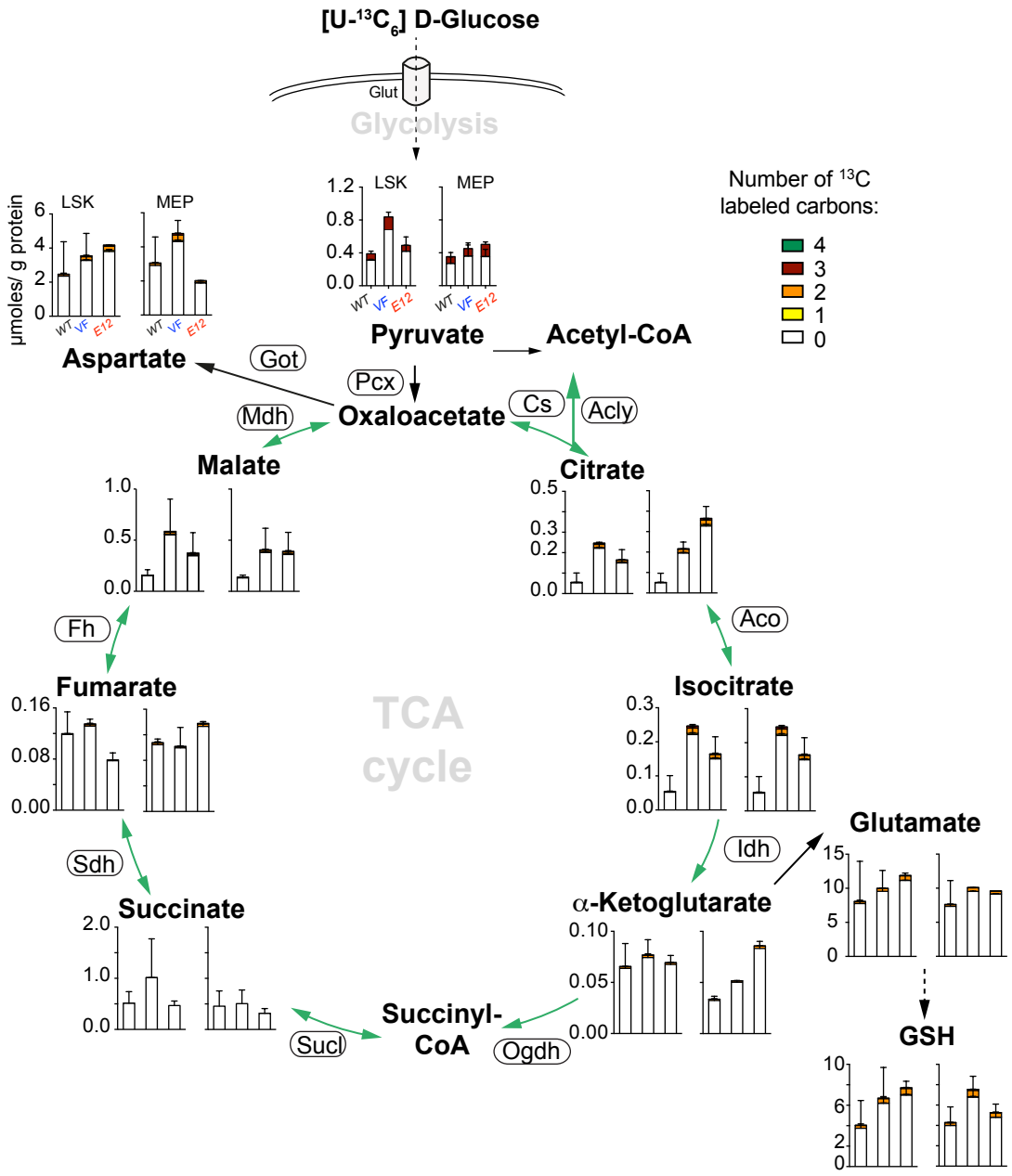

B IC-TFMS based tracing of incorporated ^{13}C from U-$^{13}C_6$ D-glucose in purine/ pyrimidine pathway metabolites in LSK and MEP cells

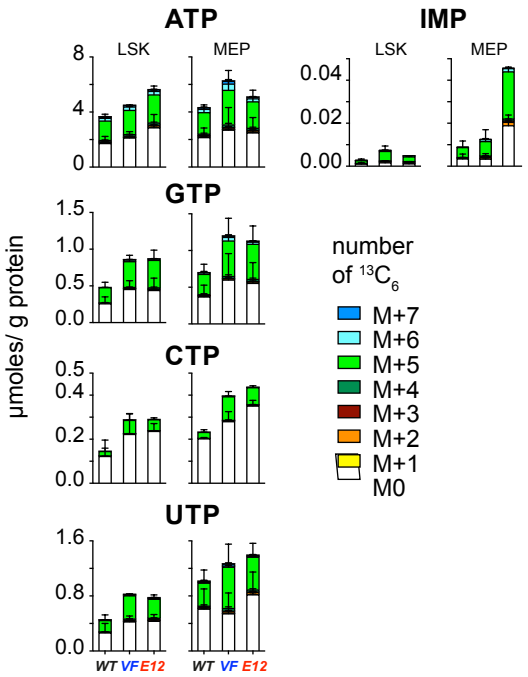

C Expression levels of PPP and nucleotide synthesis pathway genes in bone marrow MEP cells

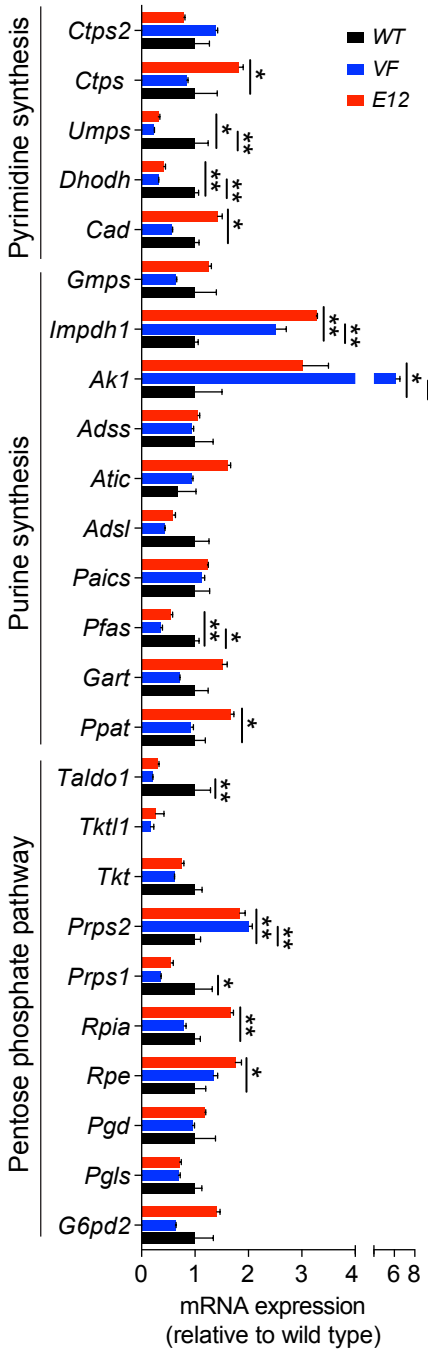

Supplemental Figure S6

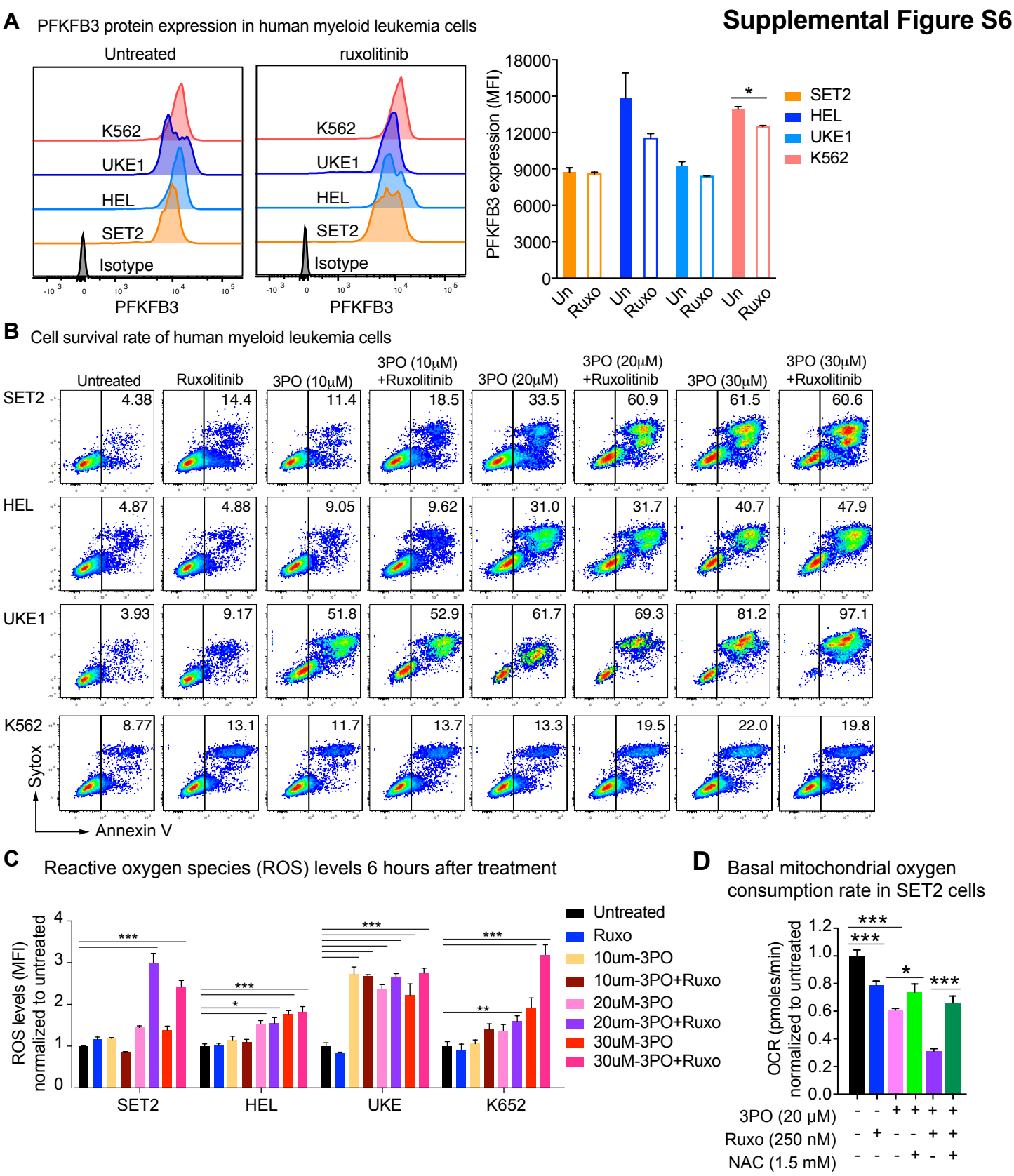

Supplemental Figure S6. Dual treatment with 3PO and ruxolitinib induces cell proliferation arrest and apoptosis in human leukemic cell lines by evoking ROS levels. (A) Pfkfb3 protein expression in human myeloid leukemia cells (SET2, HEL UKE1, and K562) as determined by flow cytometry after vehicle or ruxolitinib treatment for 24h and shown as representative histogram and bar chart. (B) Representative FACS plots showing the percentages of apoptotic cells after drug treatment for 48 hours (n=3). (C) Bar graph showing the ROS levels in indicated cells treated with 3PO and/or ruxolitinib for 6 hours. Data shown are normalized values of MFI (n=3). (D) Bar graph showing basal OCR levels in indicated cells treated with 3PO and/or ruxolitinib for 6 hours. Cells were pretreated with NAC for 6 hours where indicated. Data shown are normalized values of MFI (n=3 experiments). All data are presented as mean ± SEM. Unpaired Student's t tests (A) or One-way ANOVA analyses followed by Tukey's multiple comparison tests were used for multiple group comparisons (C). *P < .05; **P < .01; ***P < .001.

Supplemental Figure S7

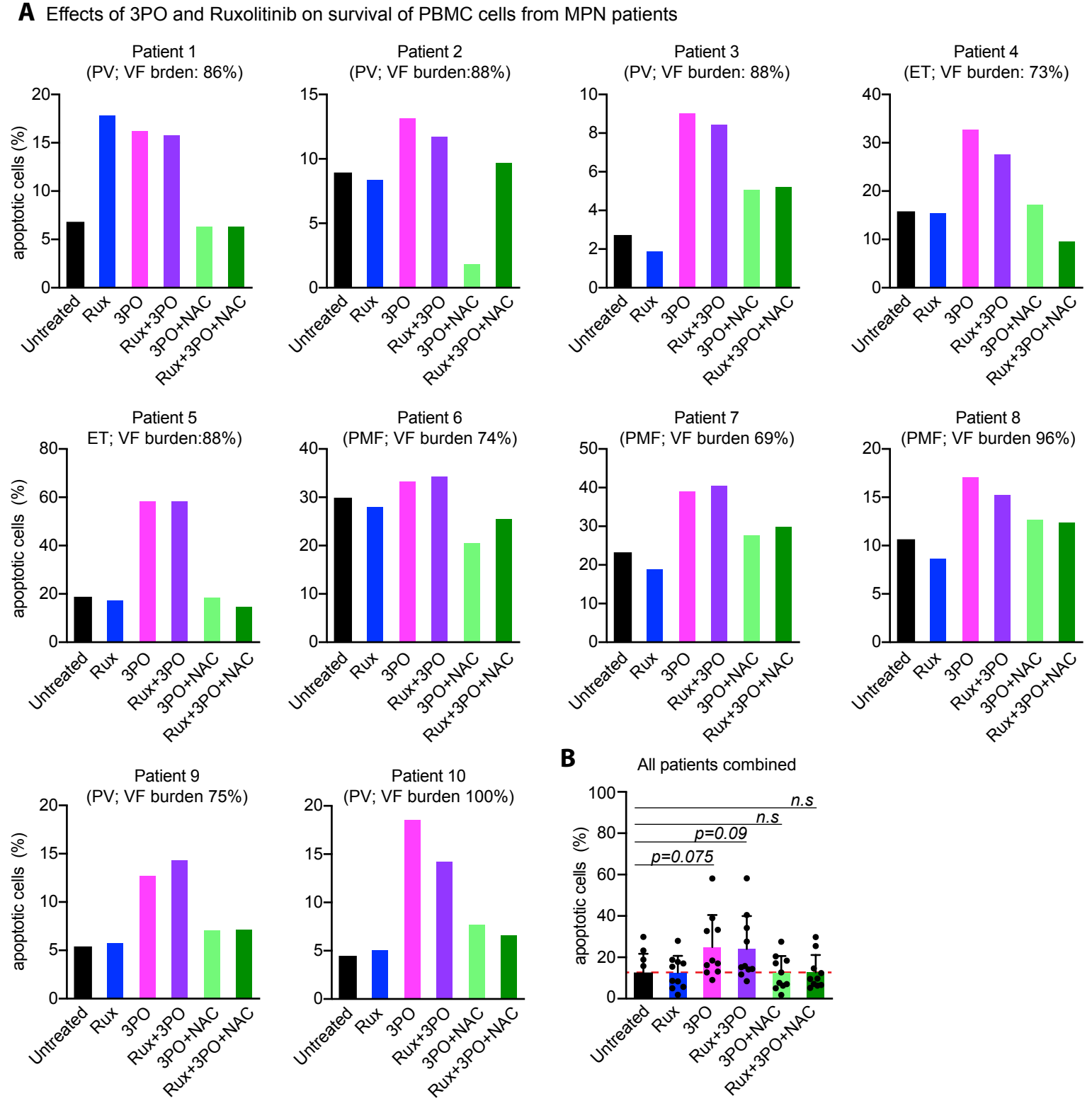

Supplemental Figure S7. Inhibition of glycolysis with Pfkfb3 inhibitor 3PO induces apoptosis in peripheral blood mononuclear cells (PBMCs) from MPN patients (n=10). A) Bar graphs show the percentages of apototic cells (Annexin V+ Sytox+) in PMBCs treated with 3PO (30μM) or Ruxolitinib (250nM) alone, or in combination for 48hours. PBMCs were pretreated with N-Acetyl-Cystein (NAC) (1.5 mM) for 6 hours where indicated. The MPN subtype and the JAK2-V617F (VF) allele burden (%) of each MPN patients are indicated in parenthesis. B) Plot showing the data of all patient samples combined. Data are presented as mean ± SD. One-way ANOVA followed by Tukey's multiple comparison tests were used. n.s: not significant.

Supplemental Figure S8

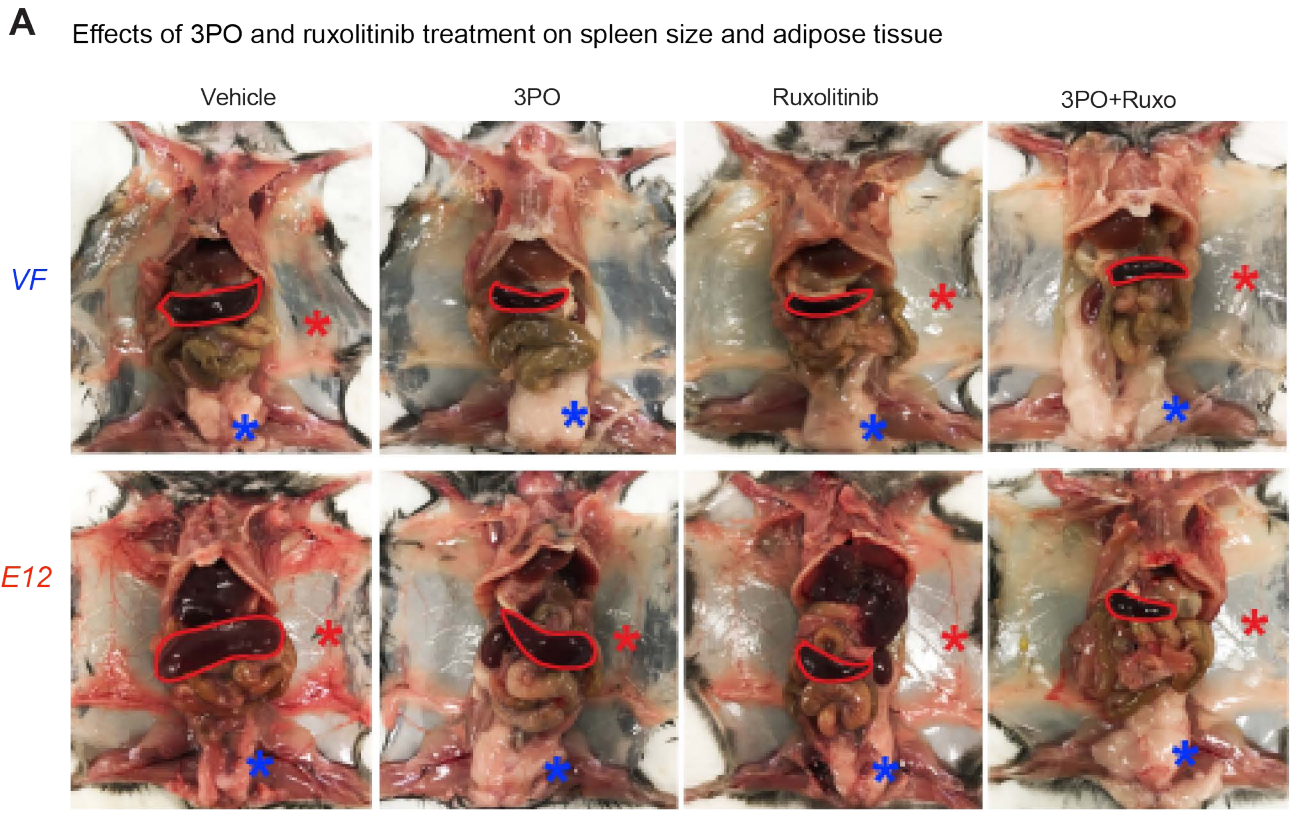

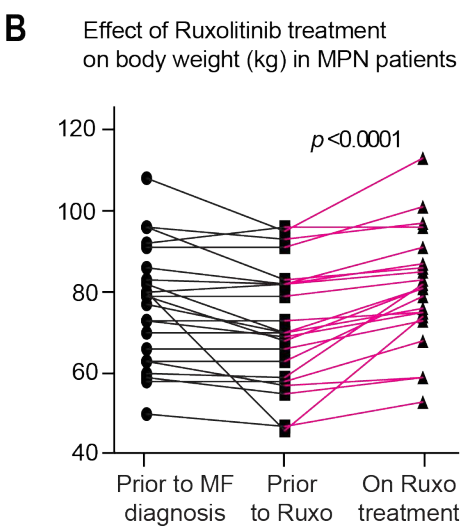

Supplemental Figure S8. Combined inhibition of Pfkfb3 activity and hyperactive JAK2 signaling ameliorates adipose atrophy in MPN mice. (A) Representative pictures of mice treated with indicated drugs for 8 weeks. Red and blue asterisks indicate subcutaneous and epididymal white adipose tissue (eWAT), respectively (n=6 mice per genotype and treatment). (B) Body weight changes in MPN patients prior to diagnosis, prior to- and during Ruxolitinib treatment. One-way ANOVA followed by Tukey's multiple comparison tests were used.